Thanatology in PPDs. Part I:

Magnetic Self-Organization in Hall-Dominated Magnetorotational Turbulence

Matthew Kunz
with Geoffroy Lesur

Protoplanetary Disks...

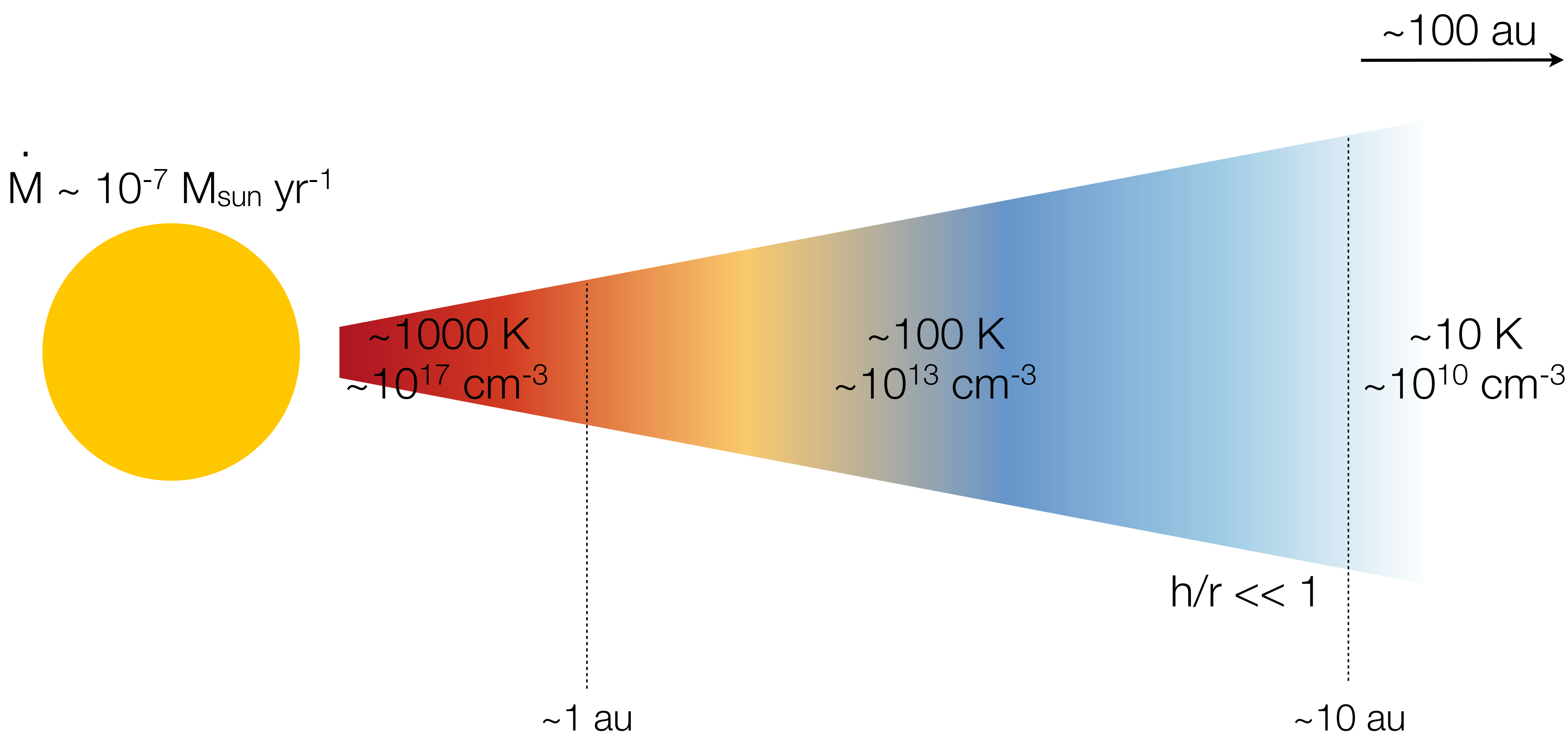

$M \sim 10^{-3} - 10^{-1}\ M_{sun}$

...are poorly ionized, casting doubt upon whether the MRI is capable of driving the observationally inferred mass-accretion rates.

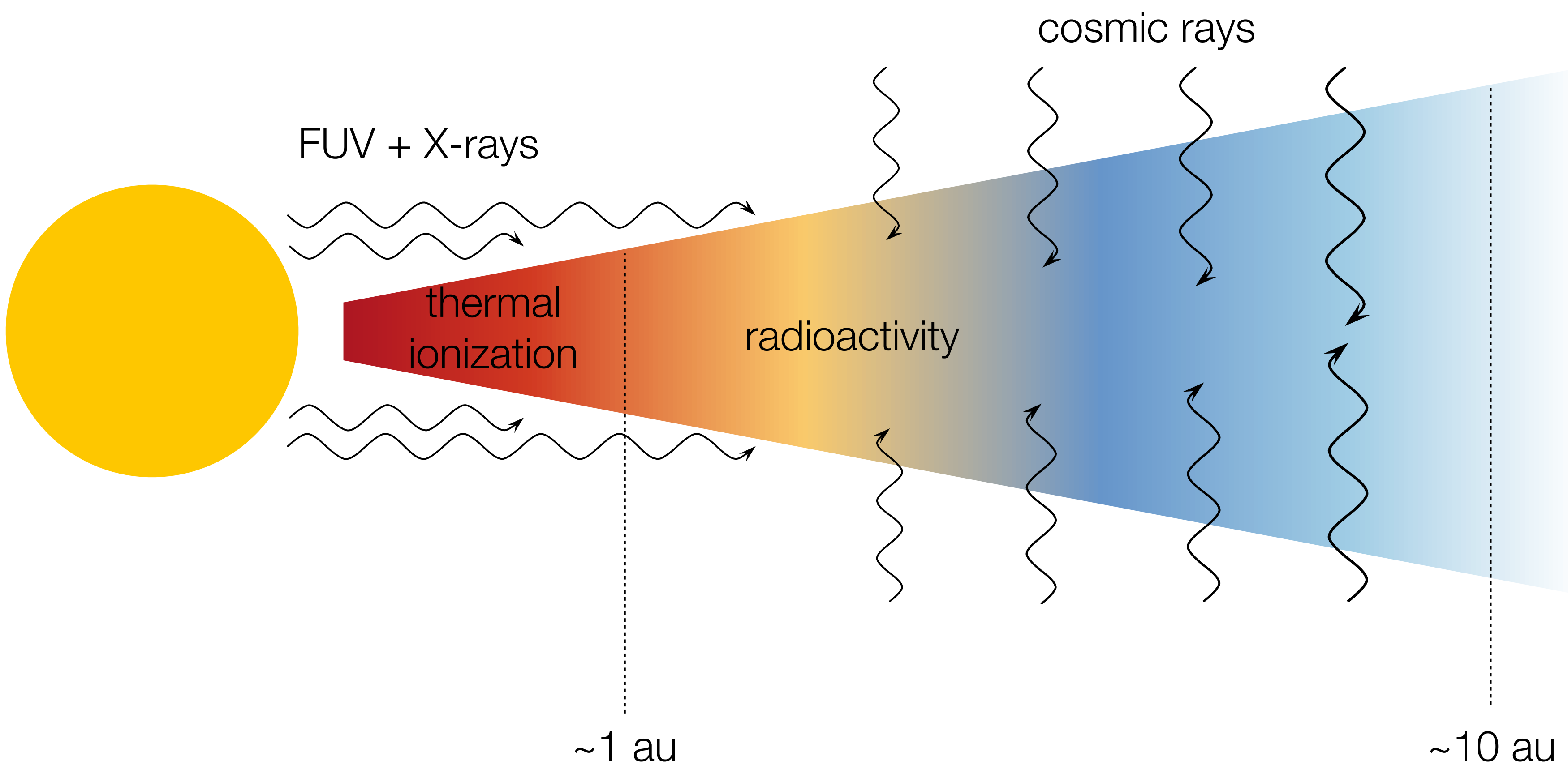

at ~1 au: $t_{\mathrm{in,coll}} \sim 3\ \mu\mathrm{s}$ $t_{\mathrm{gyr,i}} \sim 40\ \mathrm{ms}$ $t_{\mathrm{dyn}} \sim 1\ \mathrm{yr}$ $t_{\mathrm{ni,coll}} \sim 1\ \mathrm{Myr}$

$$\frac{\partial \boldsymbol{B}}{\partial t} = \boldsymbol{\nabla} \times (\boldsymbol{v}_\mathrm{f} \times \boldsymbol{B})$$

$$\frac{\partial \boldsymbol{B}}{\partial t} = \boldsymbol{\nabla} \times \Big[\qquad (\boldsymbol{v}_\mathrm{e} \qquad) \times \boldsymbol{B} + \underbrace{(\boldsymbol{v}_\mathrm{f} - \boldsymbol{v}_\mathrm{e}) \times \boldsymbol{B}}_{-\frac{4\pi\eta}{c}\boldsymbol{J}} \Big]$$

Ohmic dissipation

$$\frac{\partial \boldsymbol{B}}{\partial t} = \boldsymbol{\nabla} \times (\boldsymbol{v}_\mathrm{f} \times \boldsymbol{B})$$

$$\frac{\partial \boldsymbol{B}}{\partial t} = \boldsymbol{\nabla} \times \Big[\qquad\qquad (\boldsymbol{v}_\mathrm{i} \qquad\quad) \times \boldsymbol{B} + \underbrace{(\boldsymbol{v}_\mathrm{e} - \boldsymbol{v}_\mathrm{i})}_{-\frac{\boldsymbol{J}}{e n_\mathrm{e}}} \times \boldsymbol{B} + \underbrace{(\boldsymbol{v}_\mathrm{f} - \boldsymbol{v}_\mathrm{e})}_{-\frac{4\pi\eta}{c}\boldsymbol{J}} \times \boldsymbol{B} \Big]$$

Hall effect

Ohmic dissipation

$$\frac{\partial \boldsymbol{B}}{\partial t} = \boldsymbol{\nabla} \times (\boldsymbol{v}_{\rm f} \times \boldsymbol{B})$$

$$\frac{\partial \boldsymbol{B}}{\partial t} = \boldsymbol{\nabla} \times \Big[\boldsymbol{v}_{\rm n} \times \boldsymbol{B} + \underbrace{(\boldsymbol{v}_{\rm i} - \boldsymbol{v}_{\rm n})}_{\dfrac{\boldsymbol{J} \times \boldsymbol{B}}{c\rho\tau_{\rm ni}^{-1}}} \times \boldsymbol{B} + \underbrace{(\boldsymbol{v}_{\rm e} - \boldsymbol{v}_{\rm i})}_{-\dfrac{\boldsymbol{J}}{en_{\rm e}}} \times \boldsymbol{B} + \underbrace{(\boldsymbol{v}_{\rm f} - \boldsymbol{v}_{\rm e}) \times \boldsymbol{B}}_{-\dfrac{4\pi\eta}{c}\boldsymbol{J}} \Big]$$

ambipolar diffusion

Hall effect

Ohmic dissipation

see Kunz & Mouschovias 2009a for elastic/inelastic grain contributions

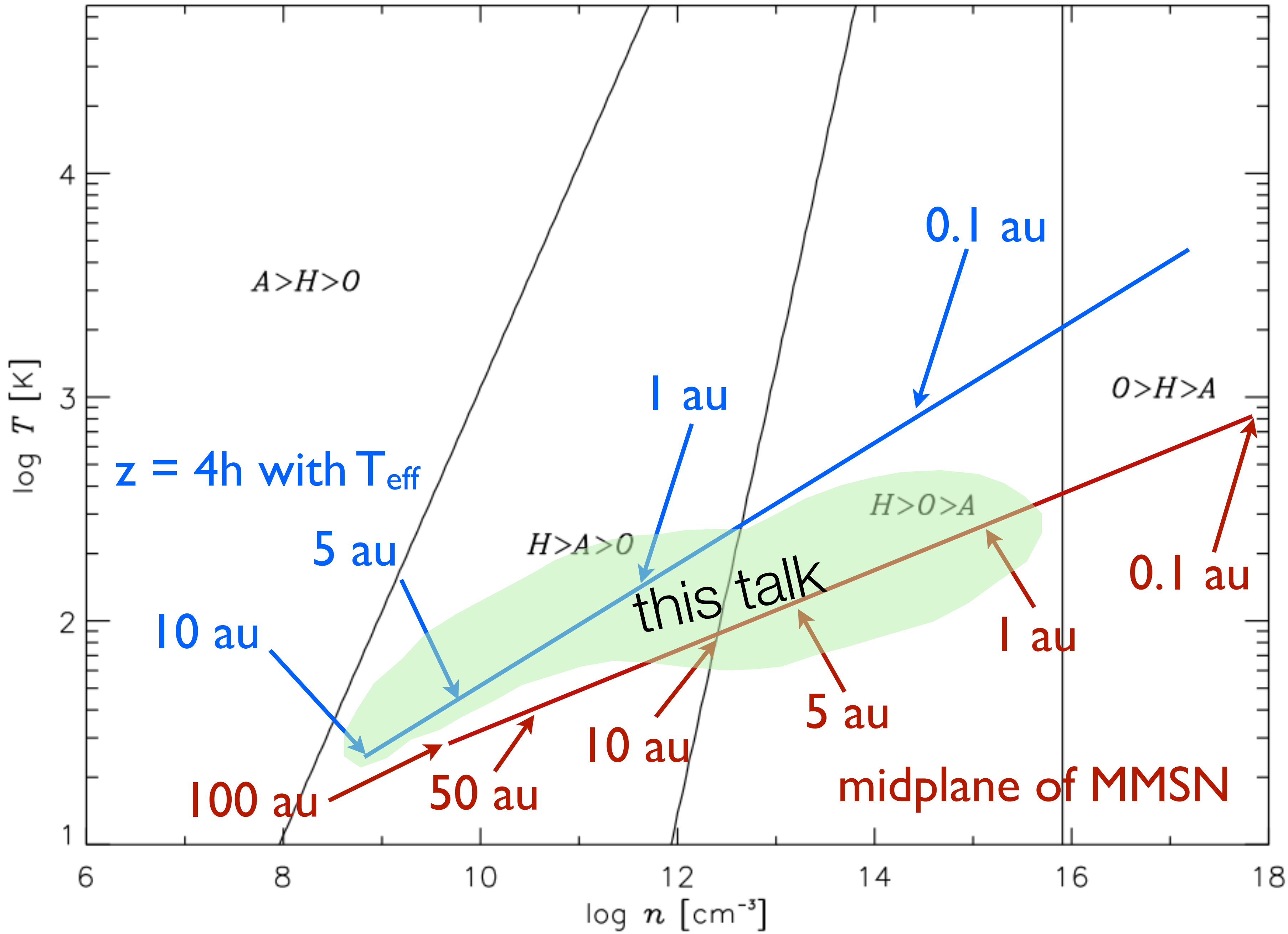

Kunz & Balbus 2004

NB: very dependent upon grain size and spatial distributions chemical network

+

disk model

=

magnetic diffusivity profiles

+

linear stability analysis

Blaes & Balbus 1994
Wardle 1999
Balbus & Terquem 2001
Kunz & Balbus 2004
Desch 2004

:

Gammie 1996
Igea & Glassgold 1999
Sano+ 2000
Salmeron & Wardle 2003, 05, 08
Wardle & Salmeron 2012

some nonlinear criterion

Fleming, Stone & Hawley 2000
Sano & Stone 2002
Bai & Stone 2011
Hawley & Stone 1998

:

Fromang+ 2002
Ilgner & Nelson 2006
Chiang & Murray-Clay 2007
Bai & Goodman 2009
Bai 2011

generically leads to *layered-accretion* model

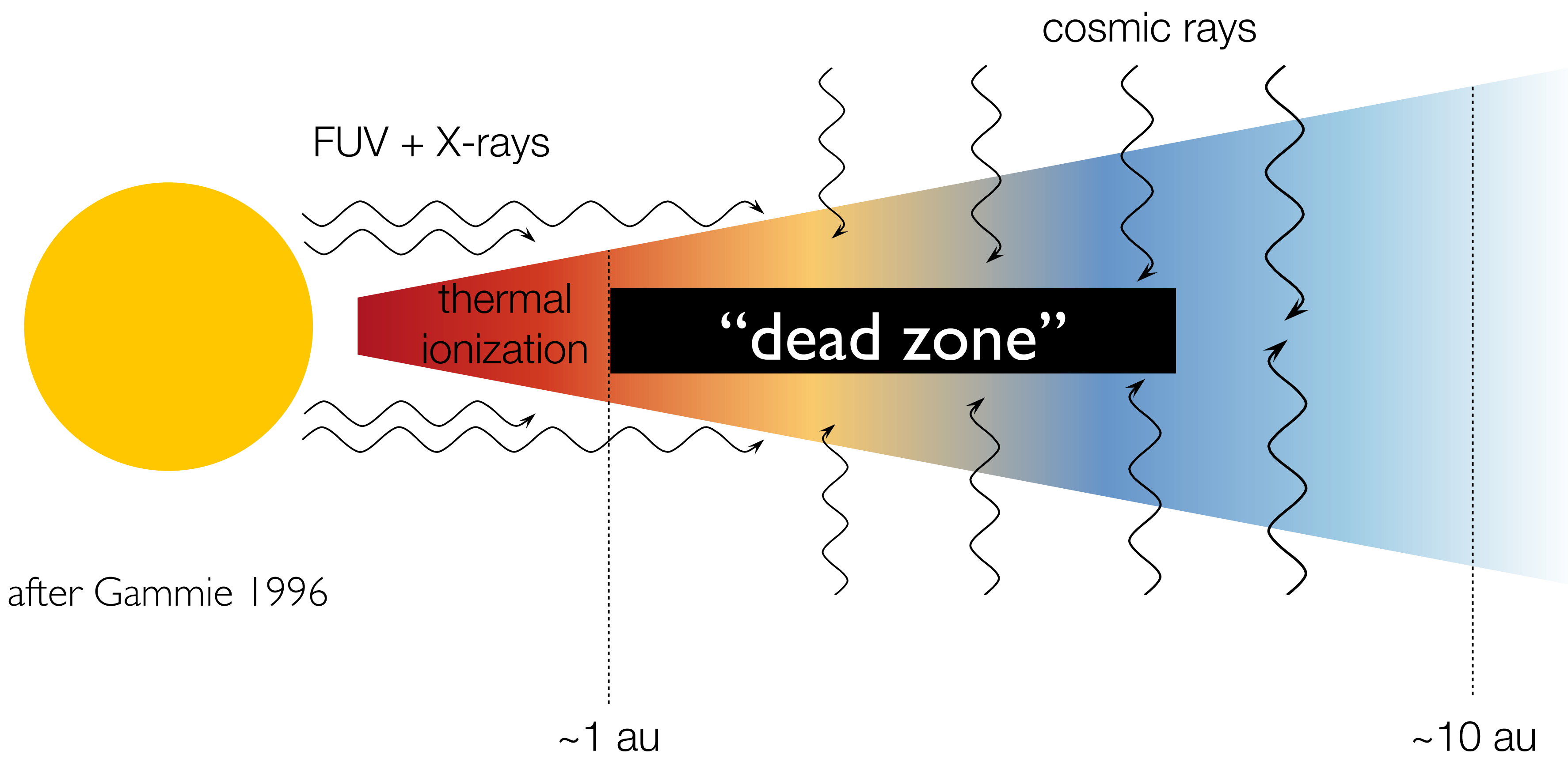

much of the PPD-MRI literature
is focused on assessing the
extent (existence?) of these zones

want them dead...

THE ORIGIN OF JOVIAN PLANETS IN PROTOSTELLAR DISKS: THE ROLE OF DEAD ZONES

Soko Matsumura and Ralph E. Pudritz

want them alive...

SELF-SUSTAINED IONIZATION AND VANISHING DEAD ZONES IN PROTOPLANETARY DISKS

Shu-ichiro Inutsuka[1] and Takayoshi Sano[2]

want them resurrected...

Breathing Life Into Dead-Zones

Orkan M. Umurhan[1,2a], Richard P. Nelson[2] and Oliver Gressel[3]

want them on life support...

DEAD ZONE ACCRETION FLOWS IN PROTOSTELLAR DISKS

N. J. Turner[1] and T. Sano[2]

want them to be zombies...

DEAD, UNDEAD, AND ZOMBIE ZONES IN PROTOSTELLAR DISKS AS A FUNCTION OF STELLAR MASS

Subhanjoy Mohanty[1], Barbara Ercolano[2,3], and Neal J. Turner[4]

From Wikipedia, the free encyclopedia

Thanatology is the scientific study of death. It investigates the mechanisms and forensic aspects of death, such as bodily changes that accompany death and the post-mortem period

θανατος

$$\Lambda_{\rm AD} \equiv (\Omega\tau_{\rm ni})^{-1} = \frac{v_{\rm A}^2}{\eta_{\rm AD}\Omega} \left(\equiv \mathrm{Am}\right)$$

linear: Blaes & Balbus 1994; Kunz & Balbus 2004; Desch 2004
nonlinear: Mac Low+1995; Hawley & Stone 1998;
Brandenburg+ 2005; Bai & Stone 2011; Simon+ 2013

Bai & Stone 2011

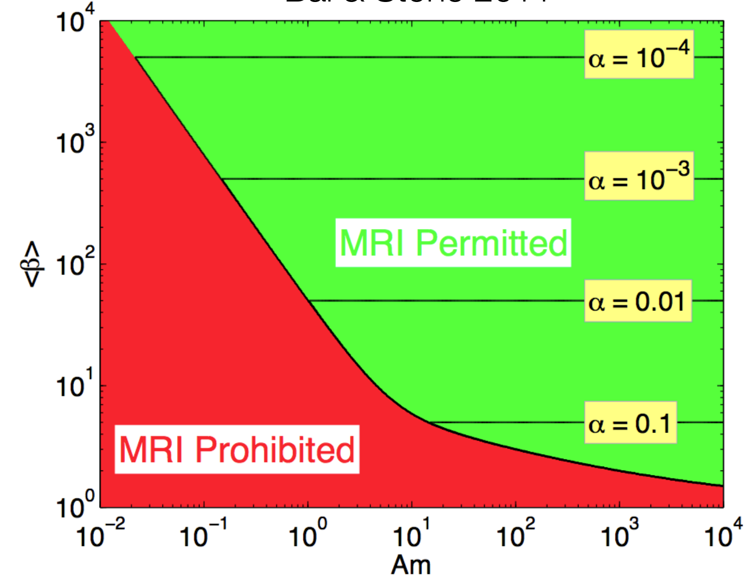

$$\Lambda_\eta \equiv (\Omega\tau_\eta)^{-1} = \frac{v_{\rm A}^2}{\eta\Omega} \left(\equiv \mathrm{Re_M}\right)$$

linear: Jin 1996; Sano & Miyama 1999; Wardle 1999
nonlinear: Fleming+ 2000; Sano & Stone 2002

Sano & Stone 2002

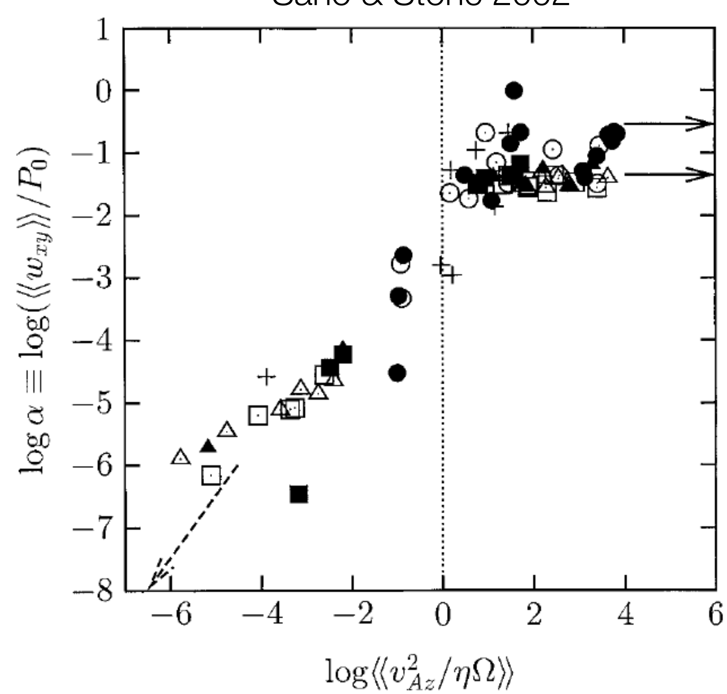

$$\Lambda_{\mathrm{H}} \equiv (\Omega \tau_{\mathrm{H}})^{-1} = \frac{v_{\mathrm{A}}^2}{\eta_{\mathrm{H}} \Omega}$$

linear: Wardle 1999; Balbus & Terquem 2001; Wardle & Salmeron 2012
nonlinear: Sano & Stone 2002

$$\tau_{\mathrm{H}} \equiv \frac{mc}{eB} \frac{n}{n_{\mathrm{e}}}$$

Sano & Stone 2002

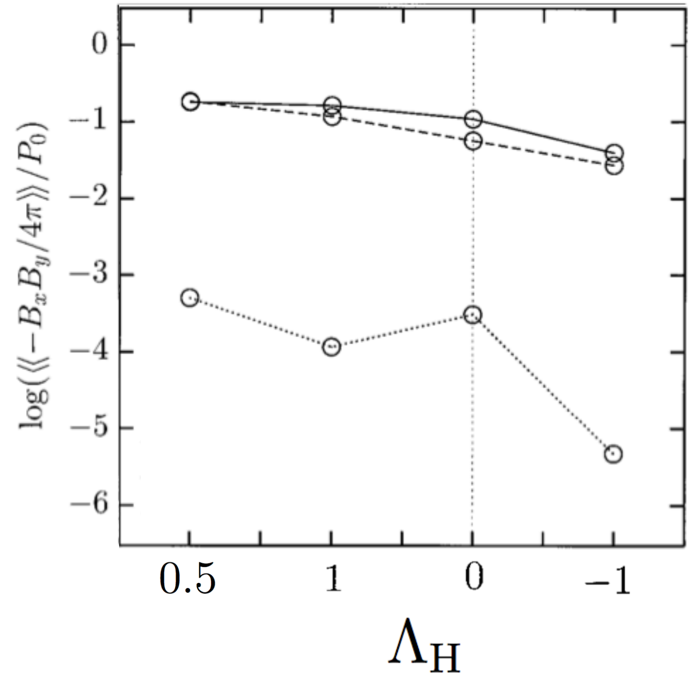

perhaps a more useful number is ℓ_{H}/H

$$\ell_{\mathrm{H}} \equiv v_{\mathrm{A}} \tau_{\mathrm{H}} = \left(\frac{m_{\mathrm{i}} c^2}{4\pi Z^2 e^2 n_{\mathrm{i}}} \right)^{1/2} \left(\frac{\rho}{\rho_{\mathrm{i}}} \right)^{1/2}$$

MMSN midplane at 10 au, B = 10 mG, *um* grains

Salmeron & Wardle 2008

ambipolar diffusion

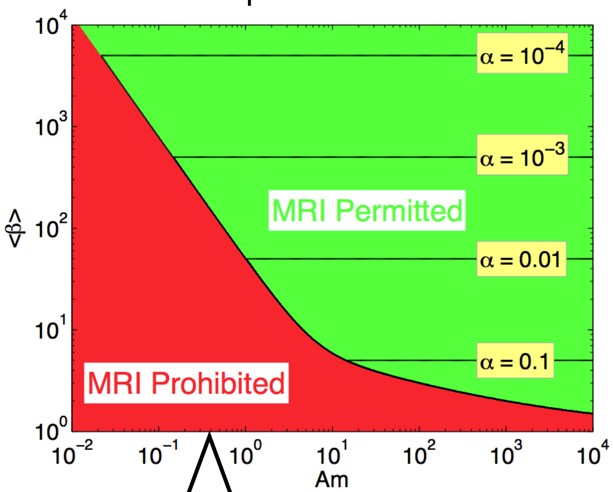

Ohmic diffusion

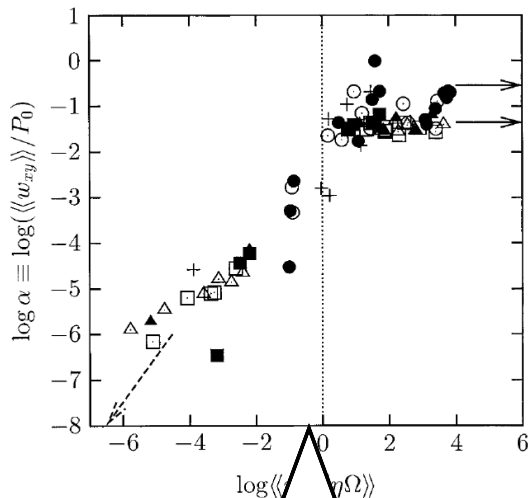

Hall diffusion

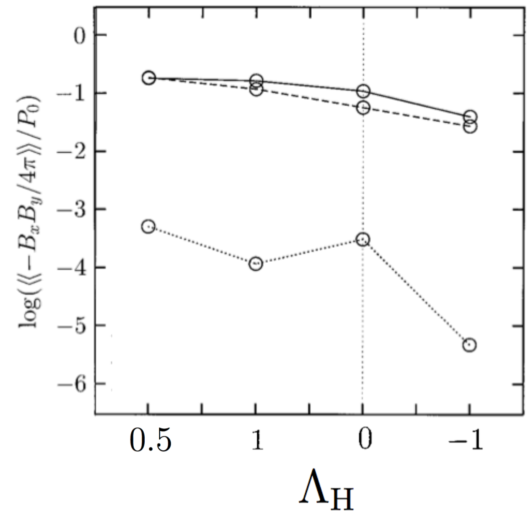

$$\Lambda_{\rm H} \sim 0.01$$

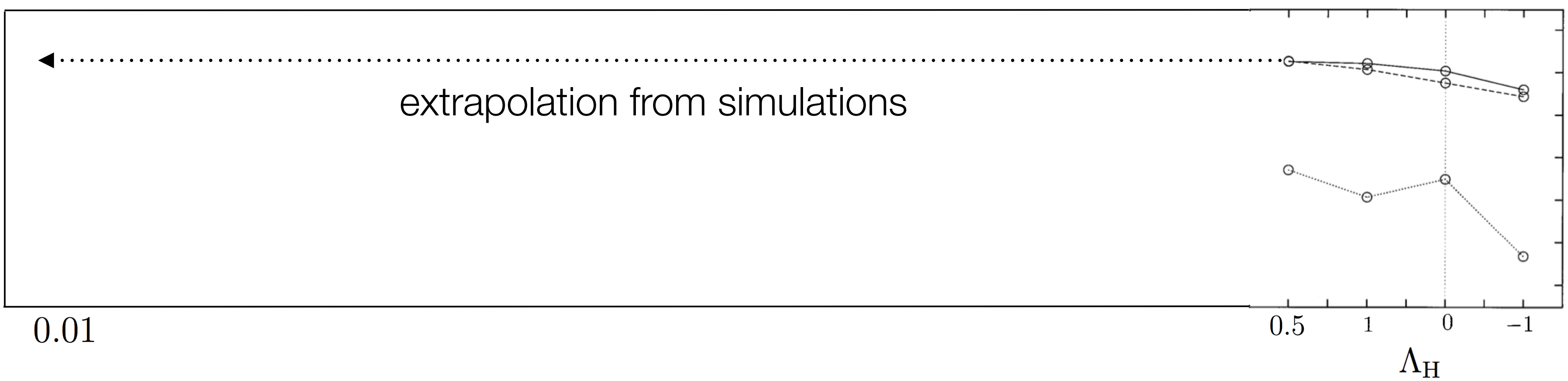

Caution from linear analysis

Wardle & Salmeron 2013

“Hall diffusion increases or decreases the MRI-active column density by an order of magnitude or more...”

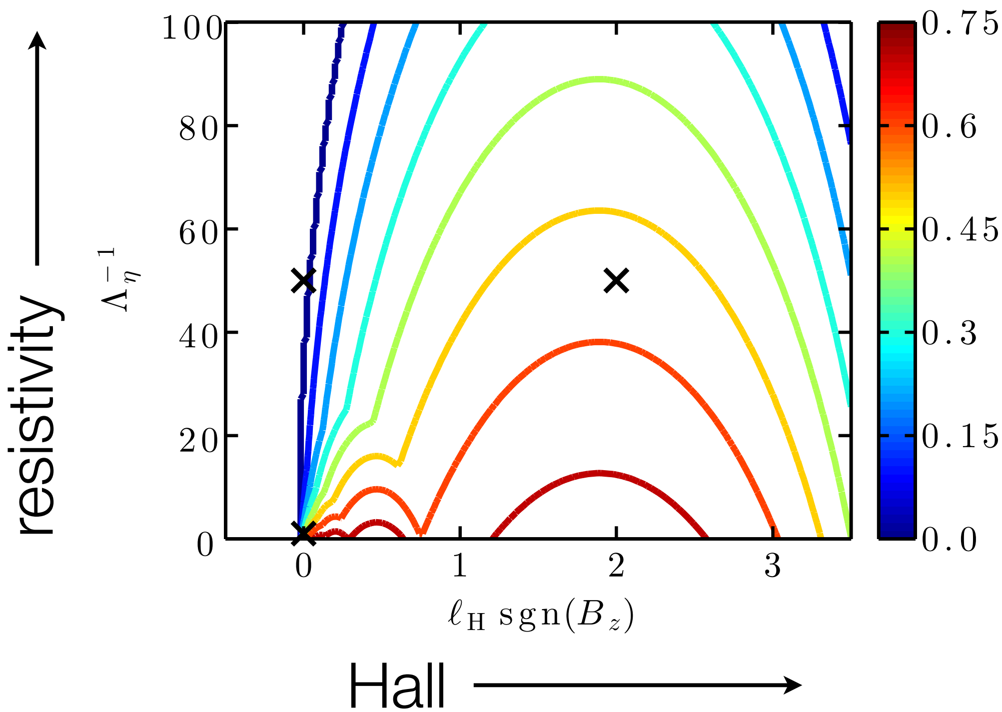

“...while the use of the linear analysis to predict the boundary of the manifestly nonlinear active region appears to be justified for the ohmic [and ambipolar] case[s], it is not known whether this applies in the Hall-dominated regime that we tout here.”

We forego a detailed study of disk chemistry and instead concentrate on turbulent dynamics themselves

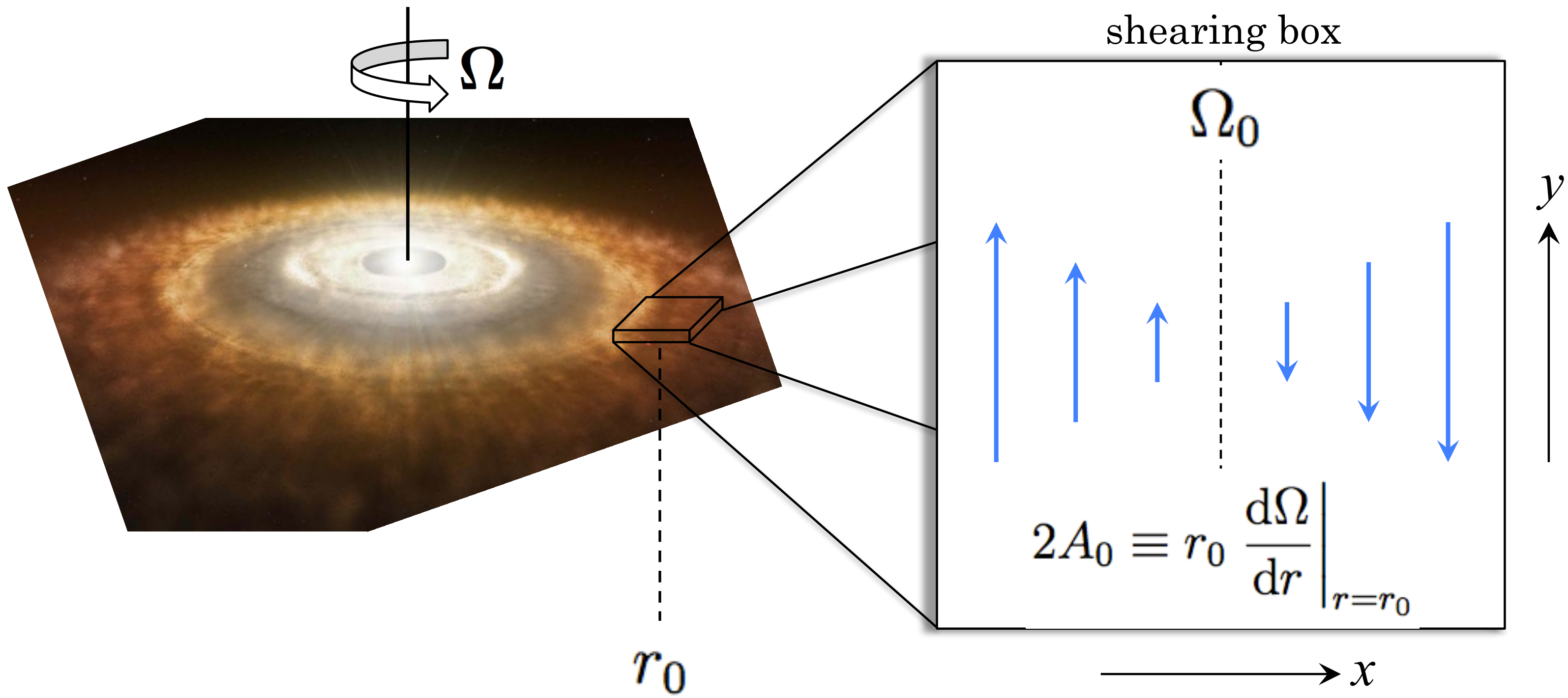

Hall (and ambipolar diffusion) added to Snoopy code

before we proceed...

1. $$\frac{\partial \boldsymbol{\omega}}{\partial t} = \boldsymbol{\nabla}\times\left(\boldsymbol{v}\times\boldsymbol{\omega} + \frac{\boldsymbol{J}\times\boldsymbol{B}}{c\rho}\right) + \nu\nabla^2\boldsymbol{\omega}$$

$$\frac{\partial \boldsymbol{B}}{\partial t} = \boldsymbol{\nabla}\times\left(\boldsymbol{v}\times\boldsymbol{B} - \frac{\boldsymbol{J}\times\boldsymbol{B}}{en_{\mathrm{e}}}\right) + \eta\nabla^2\boldsymbol{B}$$

add these:

$$\frac{\partial}{\partial t}\underbrace{\left(\boldsymbol{\omega} + \frac{e\boldsymbol{B}}{mc}\frac{n_{\mathrm{e}}}{n}\right)}_{\frac{1}{m}\boldsymbol{\nabla}\times\left[m\left(\boldsymbol{v}+\boldsymbol{\Omega}\times\boldsymbol{r}\right)+\frac{e\boldsymbol{A}}{c}\frac{n_{\mathrm{e}}}{n}\right]} = \boldsymbol{\nabla}\times\left[\boldsymbol{v}\times\left(\boldsymbol{\omega} + \frac{e\boldsymbol{B}}{mc}\frac{n_{\mathrm{e}}}{n}\right)\right] + \nabla^2\left(\nu\boldsymbol{\omega} + \eta\frac{e\boldsymbol{B}}{mc}\frac{n_{\mathrm{e}}}{n}\right)$$

$$\equiv \frac{1}{m}\boldsymbol{\nabla}\times\wp_{\mathrm{canonical}}$$

canonical vorticity
is conserved

Kelvin’s circulation theorem
generalized for Hall-MHD

Kelvin's circulation theorem generalized for Hall-MHD:

canonical circulation is a constant

$$\Gamma_{\text{canonical}} \equiv \oint_{\mathcal{C}} \boldsymbol{\wp}_{\text{canonical}} \cdot \mathrm{d}\boldsymbol{\ell} \quad \left(= \frac{1}{m} \int_{\mathcal{S}} \boldsymbol{\omega}_{\text{canonical}} \cdot \mathrm{d}\boldsymbol{S} \right)$$

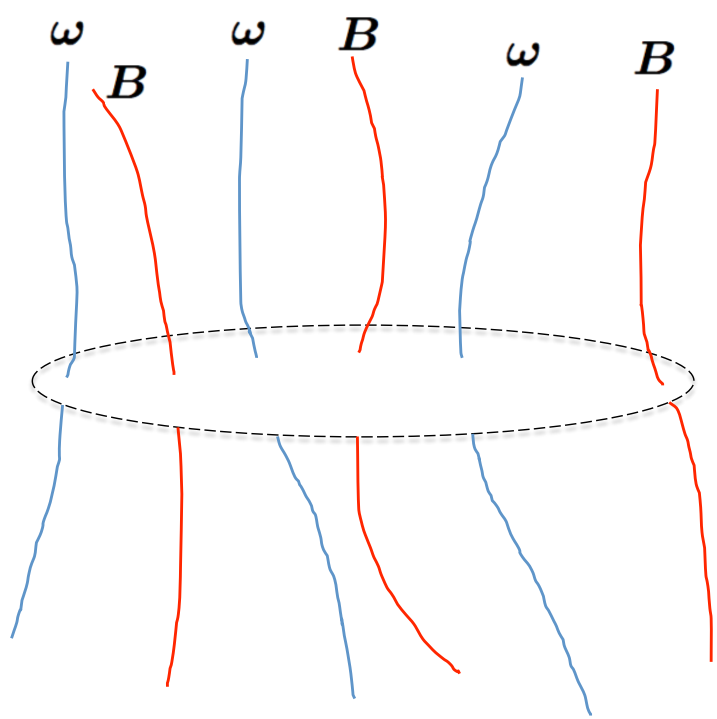

2.

$$\frac{\partial \boldsymbol{B}}{\partial t} = \boldsymbol{\nabla}\times\left(\boldsymbol{v}\times\boldsymbol{B} \underbrace{- \frac{\boldsymbol{J}\times\boldsymbol{B}}{e n_\mathrm{e}}}_{-\frac{c}{e n_\mathrm{e}}\boldsymbol{\nabla}\cdot\left(\frac{\boldsymbol{B}\boldsymbol{B}}{4\pi} - \cancel{\frac{B^2}{8\pi}\mathbf{I}}\right) = -\frac{c}{e n_\mathrm{e}}\boldsymbol{\nabla}\cdot\mathbf{M}}\right) + \eta\nabla^2\boldsymbol{B}$$

the transport of magnetic flux is intimately tied to the efficiency and nature of the angular-momentum transport

(3.)
$$\begin{aligned} \boldsymbol{B} &= \boldsymbol{B}_0 + \boldsymbol{B}_{\mathrm{ch}} \\ &= B_0 \hat{\boldsymbol{e}}_z + b e^{\gamma t} B_0 \cos Kz \left(\hat{\boldsymbol{e}}_x \sin\theta - \hat{\boldsymbol{e}}_y \cos\theta \right) \end{aligned}$$

$$\begin{aligned} \boldsymbol{v} &= \boldsymbol{v}_0 + \boldsymbol{v}_{\mathrm{ch}} \\ &= 2Ax \hat{\boldsymbol{e}}_y + b e^{\gamma t} v_0 \sin Kz \left(\hat{\boldsymbol{e}}_x \cos\phi + \hat{\boldsymbol{e}}_y \sin\phi \right) \end{aligned}$$

$$\boldsymbol{v}_{\mathrm{ch}} \cdot \nabla \boldsymbol{v}_{\mathrm{ch}} = \boldsymbol{B}_{\mathrm{ch}} \cdot \nabla \boldsymbol{B}_{\mathrm{ch}} = \boldsymbol{v}_{\mathrm{ch}} \cdot \nabla \boldsymbol{B}_{\mathrm{ch}} = \boldsymbol{B}_{\mathrm{ch}} \cdot \nabla \boldsymbol{v}_{\mathrm{ch}} = \boldsymbol{J}_{\mathrm{ch}} \cdot \nabla \boldsymbol{B}_{\mathrm{ch}} = \boldsymbol{B}_{\mathrm{ch}} \cdot \nabla \boldsymbol{J}_{\mathrm{ch}} = 0$$

channel modes are exact also in Hall-MHD

(can look at parasites, which are suppressed by Hall

... fun calculation, but doesn’t appear to matter) numerical results

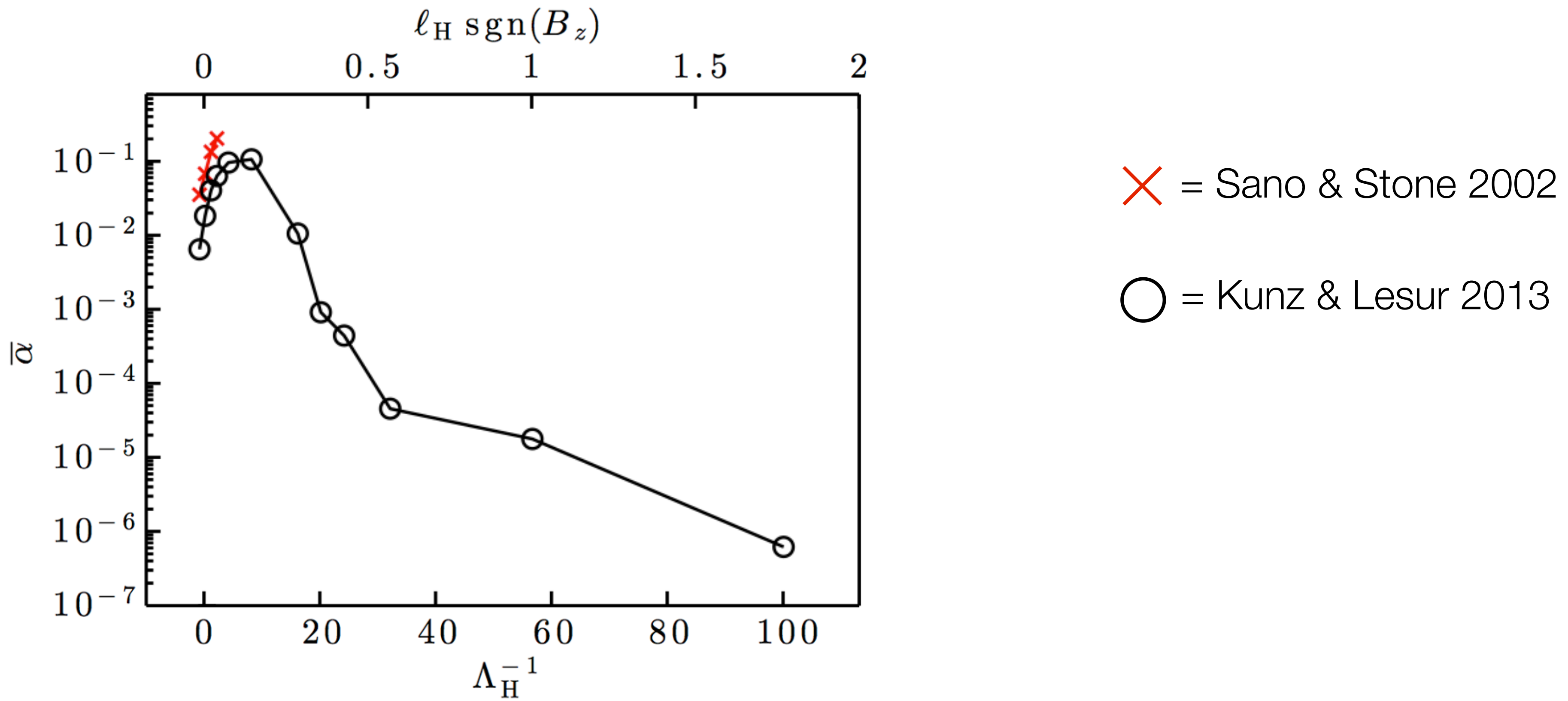

NB: The low values of transport at large Λ_H^{-1} are not due to linear stabilization vary initial beta and resistivity:

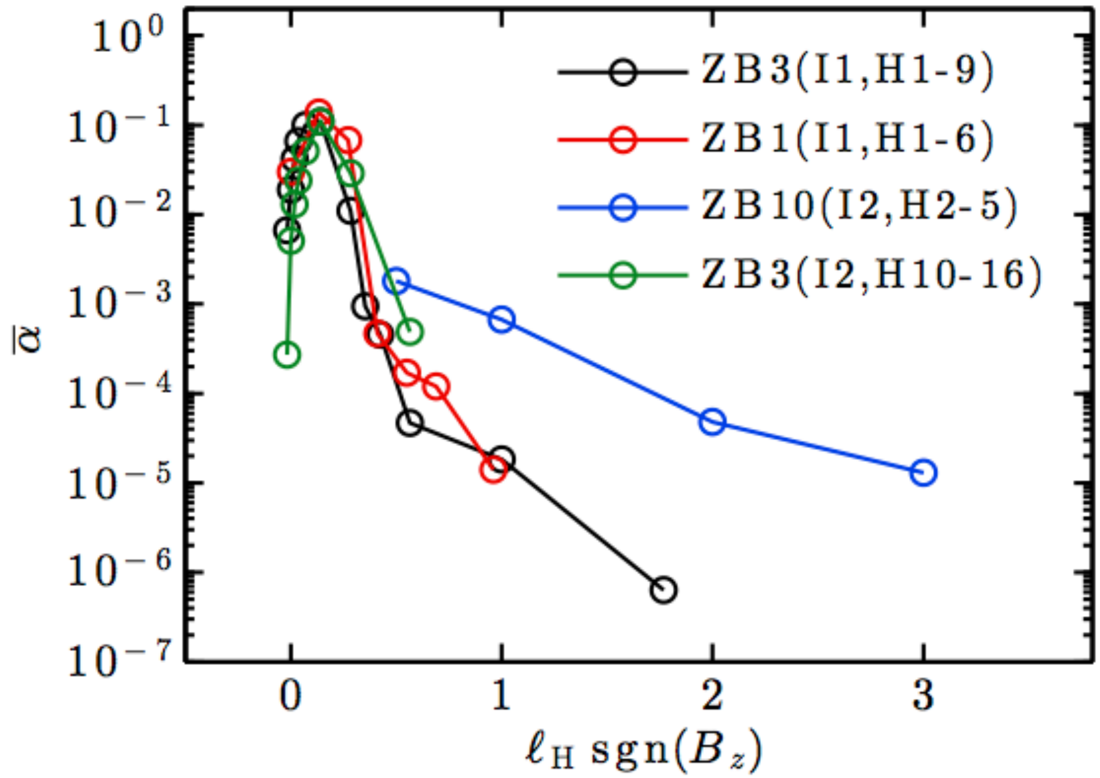

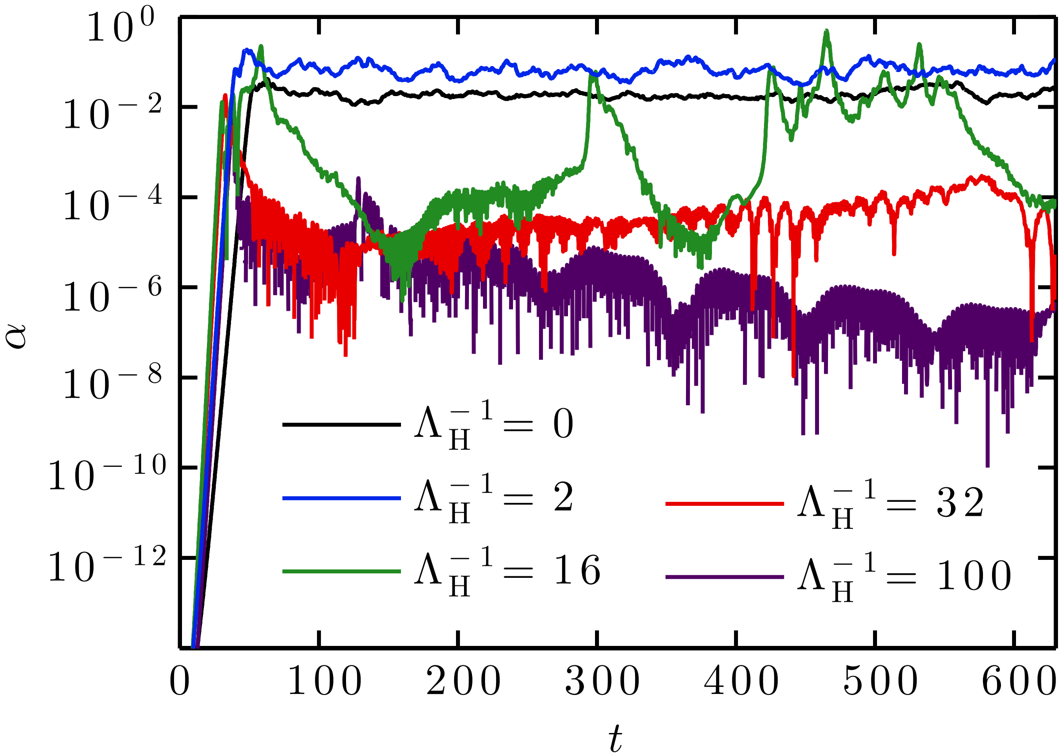

high-transport state

low-transport state

ideal MHD: high-transport state

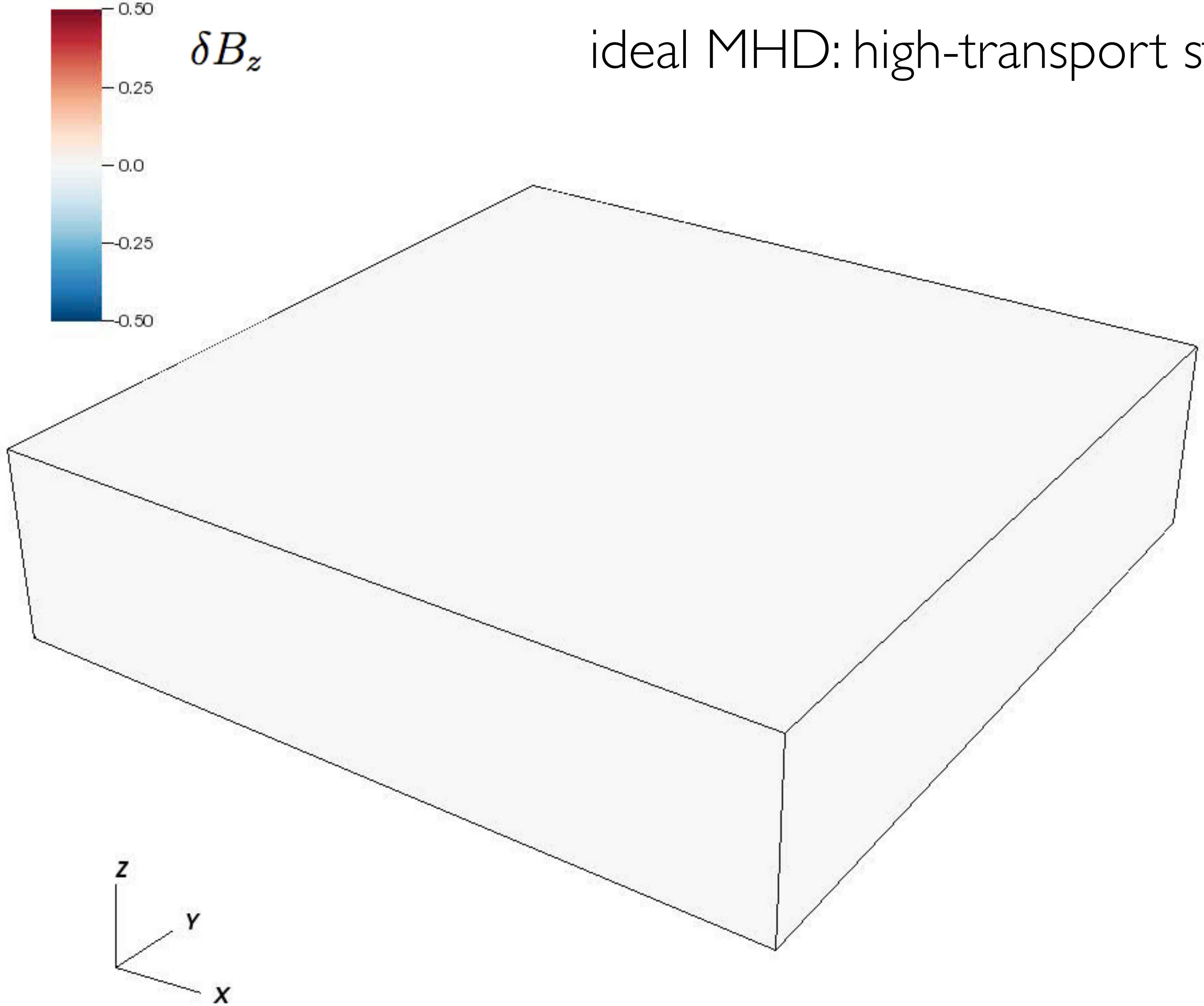

Hall-MHD: low-transport state

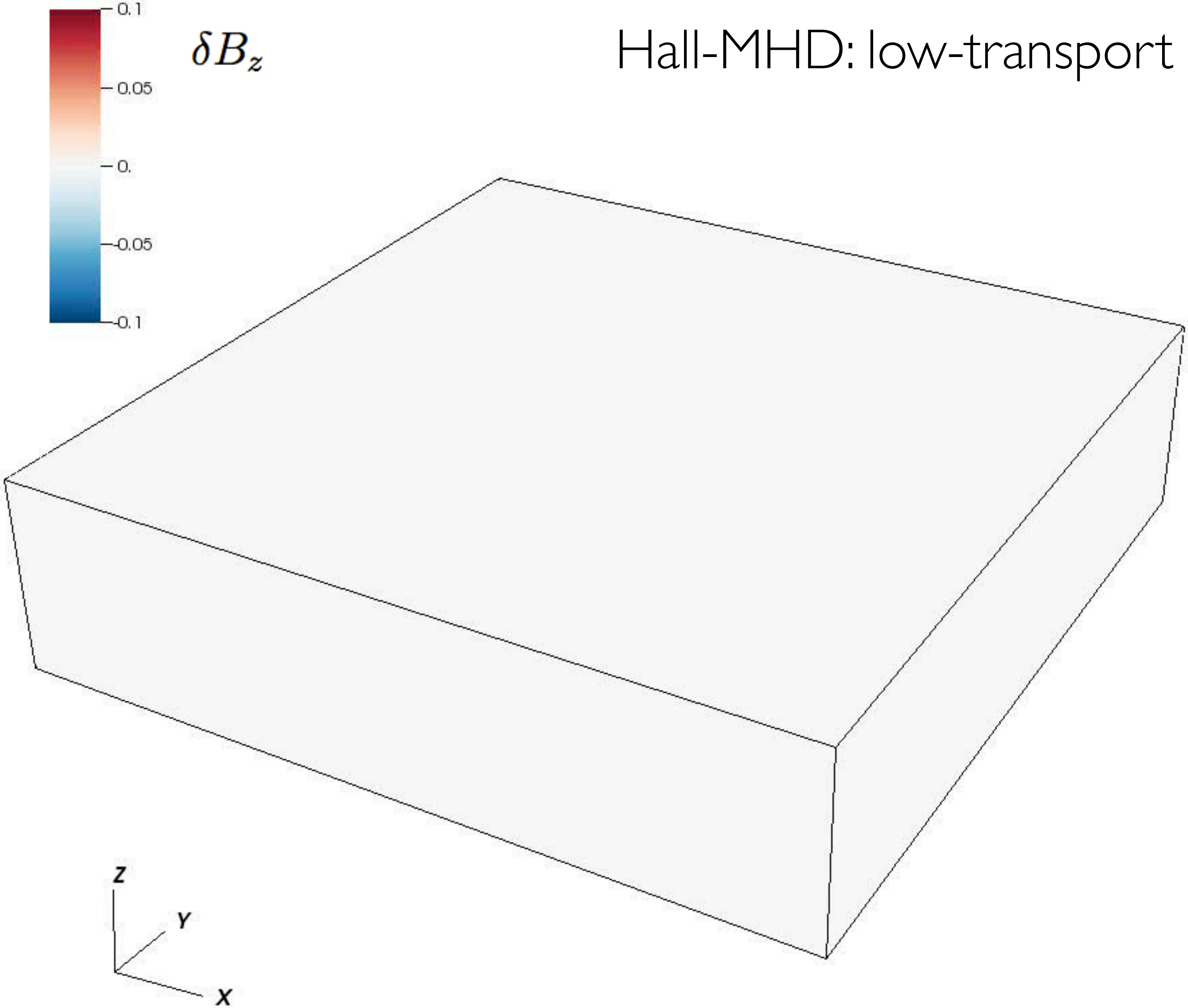

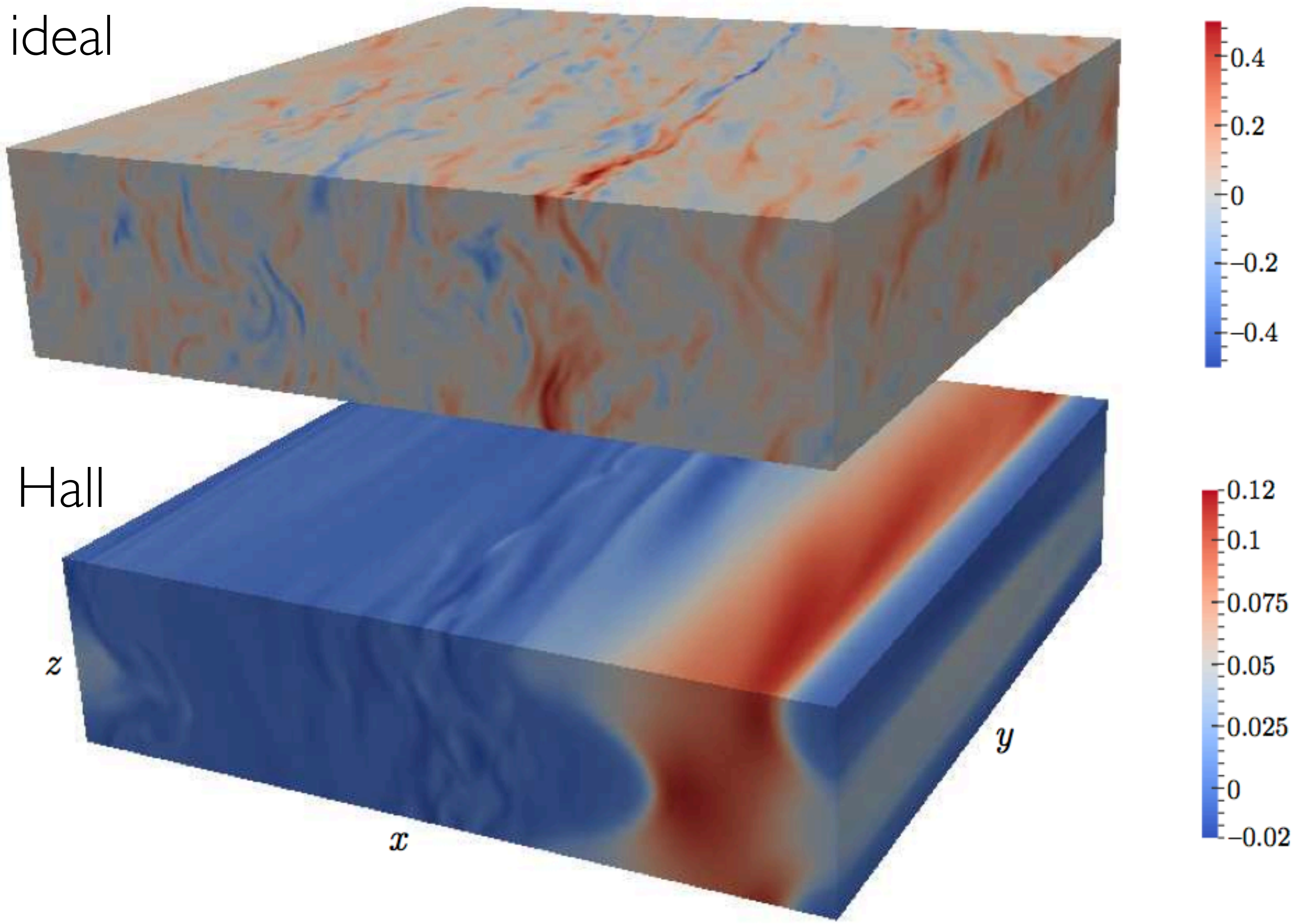
ideal
Hall
z
x
y
0.4
0.2
0
−0.2
−0.4
0.12
0.1
0.075
0.05
0.025
0
−0.02

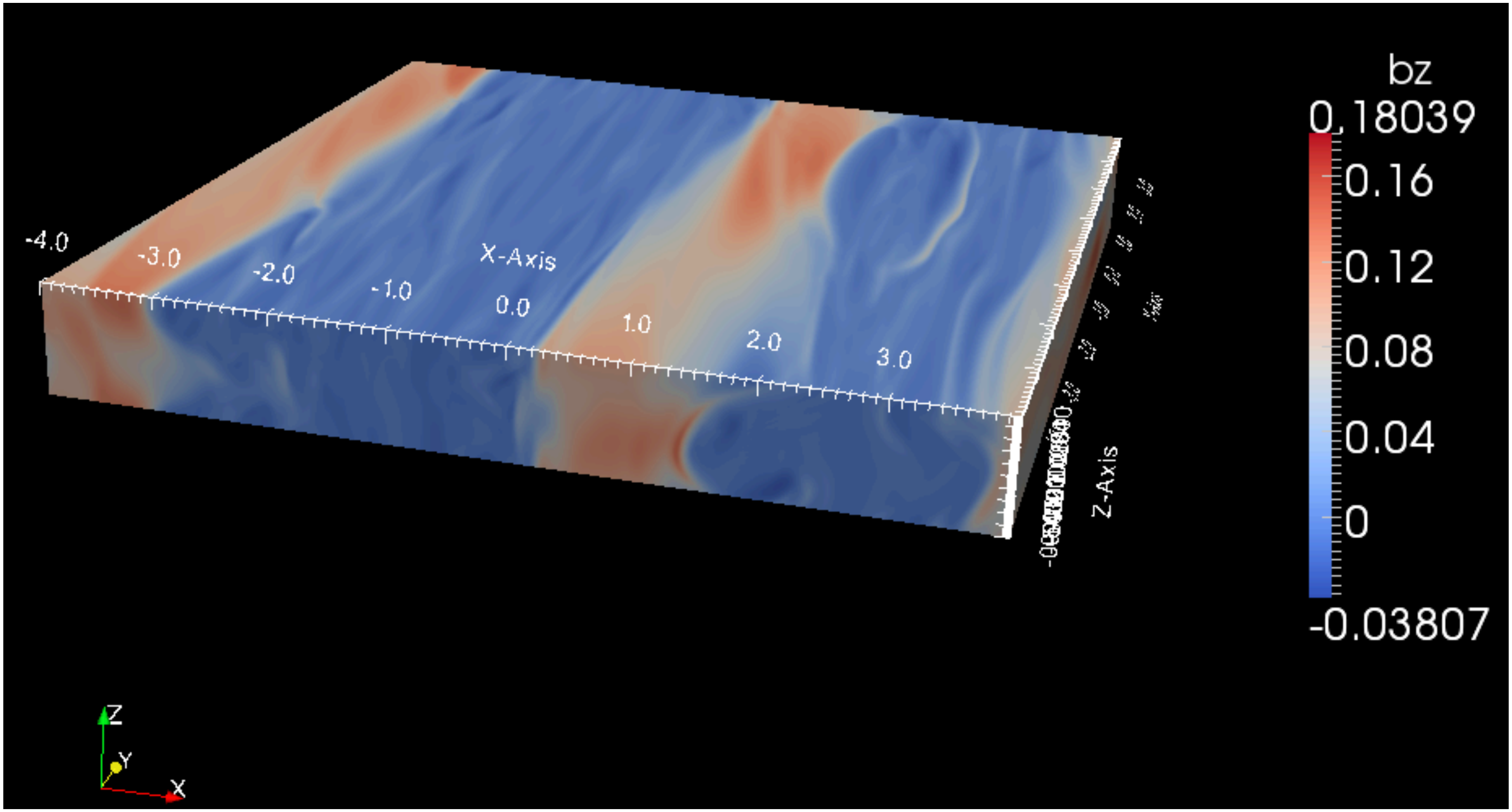

bz
0.18039
0.16
0.12
0.08
0.04
0
-0.03807
X-Axis
-4.0
-3.0
-2.0
-1.0
0.0
1.0
2.0
3.0
Z-Axis
Z
Y
X

$$\langle \cdot \rangle \equiv \frac{1}{L_y L_z} \iint \mathrm{d}y\, \mathrm{d}z$$

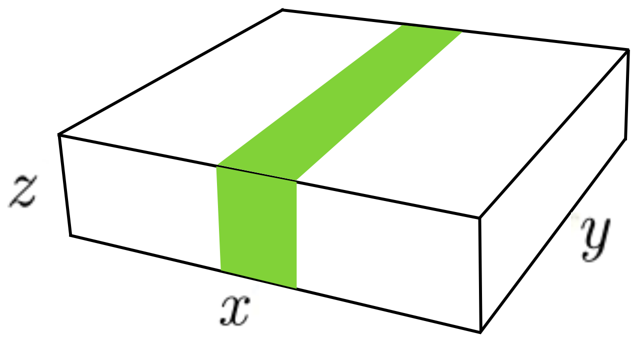

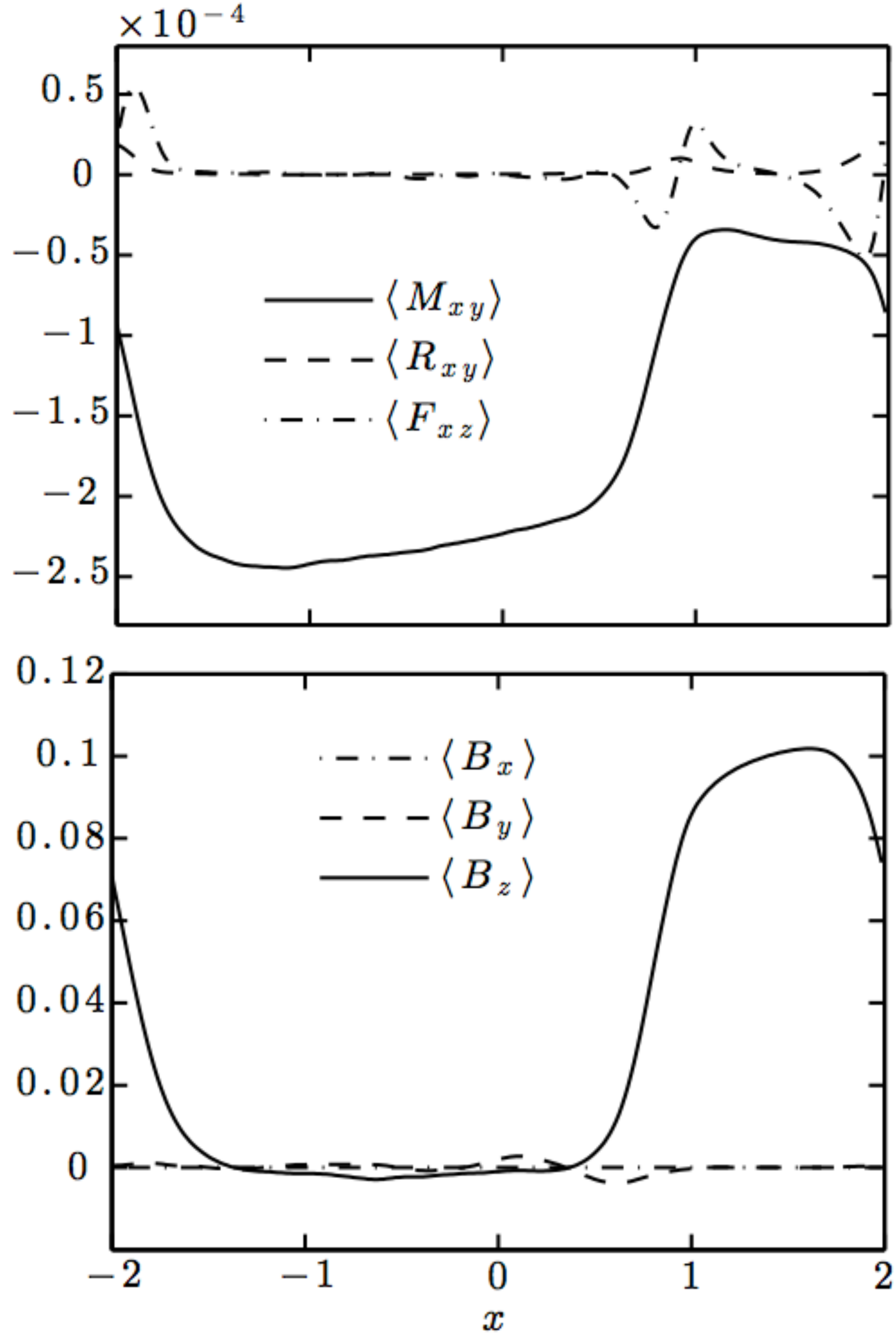

$$M_{ij} \equiv \frac{1}{4\pi} \delta B_i \delta B_j$$

$$R_{ij} \equiv \rho\, \delta v_i \delta v_j$$

$$F_{ij} \equiv \delta v_i \delta B_j - \delta v_j \delta B_i$$

mean-field model

$$\boldsymbol{v} = 2Ax\hat{\boldsymbol{y}} + \langle\boldsymbol{v}\rangle + \delta\boldsymbol{v} \quad \text{and} \quad \boldsymbol{B} = \langle\boldsymbol{B}\rangle + \delta\boldsymbol{B}$$

$$R_{ij} \equiv \rho\,\delta v_i \delta v_j \qquad M_{ij} \equiv \frac{1}{4\pi}\delta B_i \delta B_j \qquad F_{ij} \equiv \delta v_i \delta B_j - \delta v_j \delta B_i$$

$$\langle\cdot\rangle \equiv \frac{1}{L_y L_z}\iint \mathrm{d}y\,\mathrm{d}z$$

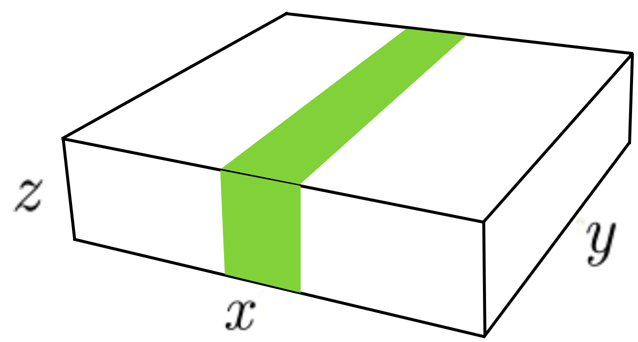

$$\frac{\partial \langle B_z \rangle}{\partial t} = -\frac{\partial \langle F_{xz} \rangle}{\partial x} - \frac{c}{e n_\mathrm{e}} \frac{\partial^2 \langle M_{xy} \rangle}{\partial x^2} + \eta \frac{\partial^2 \langle B_z \rangle}{\partial x^2}$$

Lesur & Longaretti 2009

$$\longrightarrow \quad \frac{\partial \langle B_z \rangle}{\partial t} = (\eta + \eta_\mathrm{t}) \frac{\partial^2 \langle B_z \rangle}{\partial x^2} - \frac{c}{e n_\mathrm{e}} \frac{\partial^2 \langle M_{xy} \rangle}{\partial x^2}$$

$$\frac{\partial \langle \omega_z \rangle}{\partial t} = -\frac{1}{\rho} \frac{\partial^2 \langle R_{xy} \rangle}{\partial x^2} + \frac{1}{\rho} \frac{\partial^2 \langle M_{xy} \rangle}{\partial x^2} + \nu \frac{\partial^2 \langle \omega_z \rangle}{\partial x^2}$$

$$\longrightarrow \quad \frac{\partial \langle \omega_z \rangle}{\partial t} = (\nu + \nu_\mathrm{t}) \frac{\partial^2 \langle \omega_z \rangle}{\partial x^2} + \frac{1}{\rho} \frac{\partial^2 \langle M_{xy} \rangle}{\partial x^2}$$

Case I: $\langle M_{xy} \rangle = M(\langle B_z \rangle)$

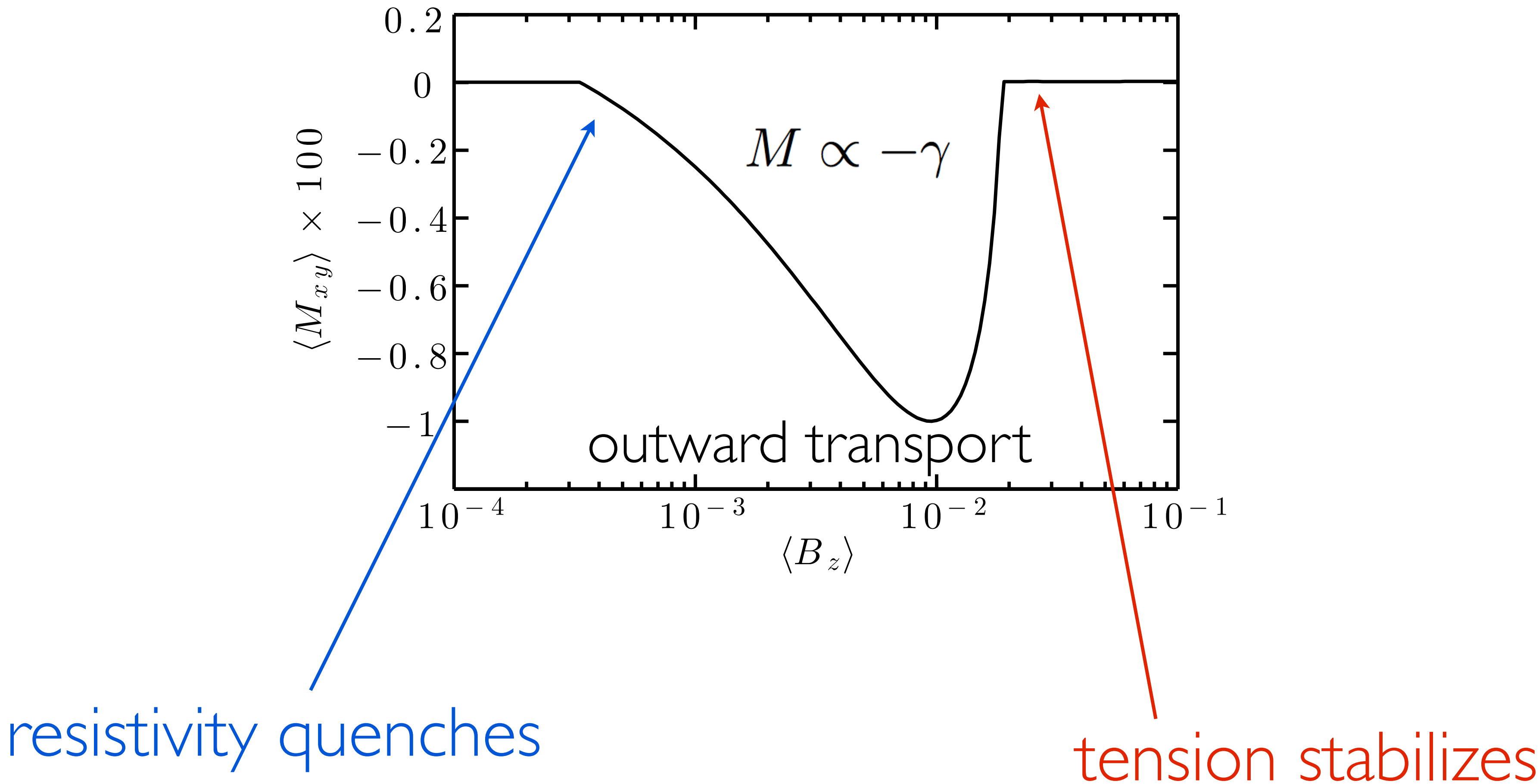

Case I: $\langle M_{xy} \rangle = M(\langle B_z \rangle)$

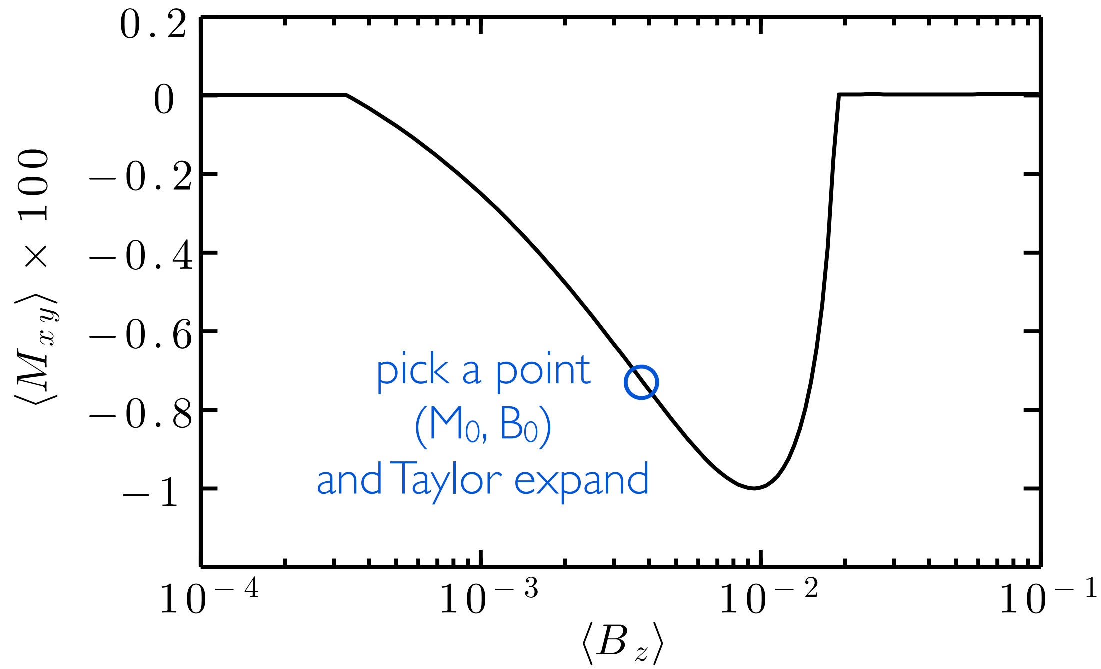

$$\frac{\mathrm{d}\langle B_z \rangle}{\mathrm{d}t} \simeq \left(\eta + \eta_\mathrm{t} - \frac{c}{e n_\mathrm{e}} \underbrace{\left. \frac{\mathrm{d}M}{\mathrm{d}\langle B_z \rangle} \right|_{B_0}}_{\text{diffusive}} \right) \frac{\partial^2 \langle B_z \rangle}{\partial x^2}$$

Case I: $\langle M_{xy}\rangle = M(\langle B_z\rangle)$

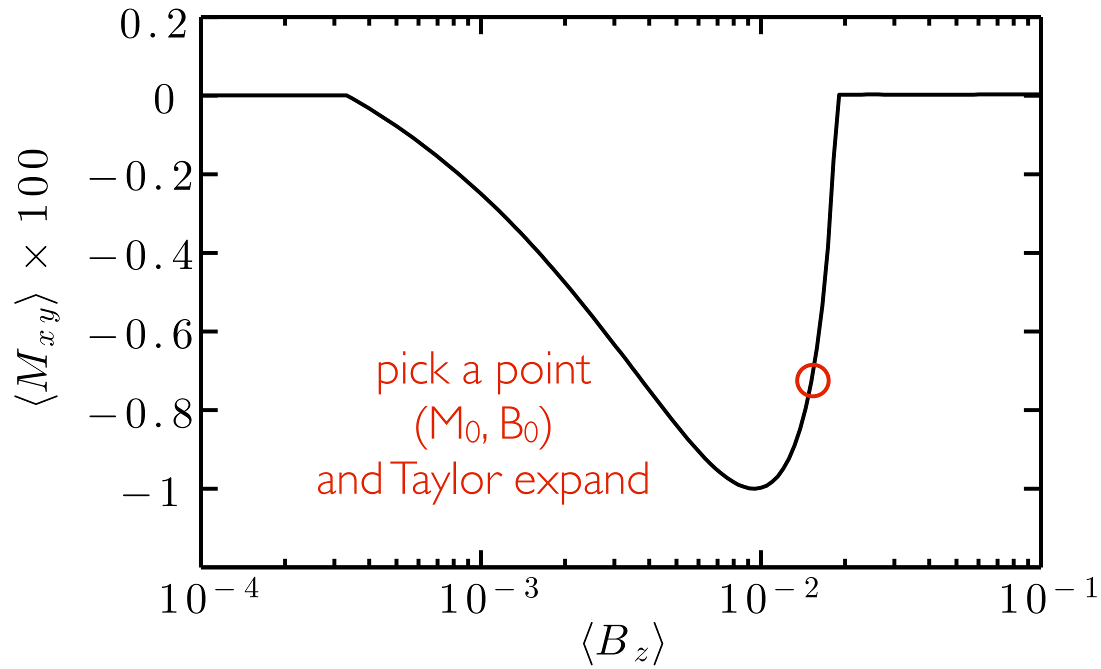

$$\frac{\mathrm{d}\langle B_z\rangle}{\mathrm{d}t} \simeq \left(\eta + \eta_{\mathrm{t}} - \frac{c}{en_{\mathrm{e}}} \underbrace{\left.\frac{\mathrm{d}M}{\mathrm{d}\langle B_z\rangle}\right|_{B_0}}_{\text{anti-diffusive}}\right) \frac{\partial^2 \langle B_z\rangle}{\partial x^2}$$

mean-field model

simulation results

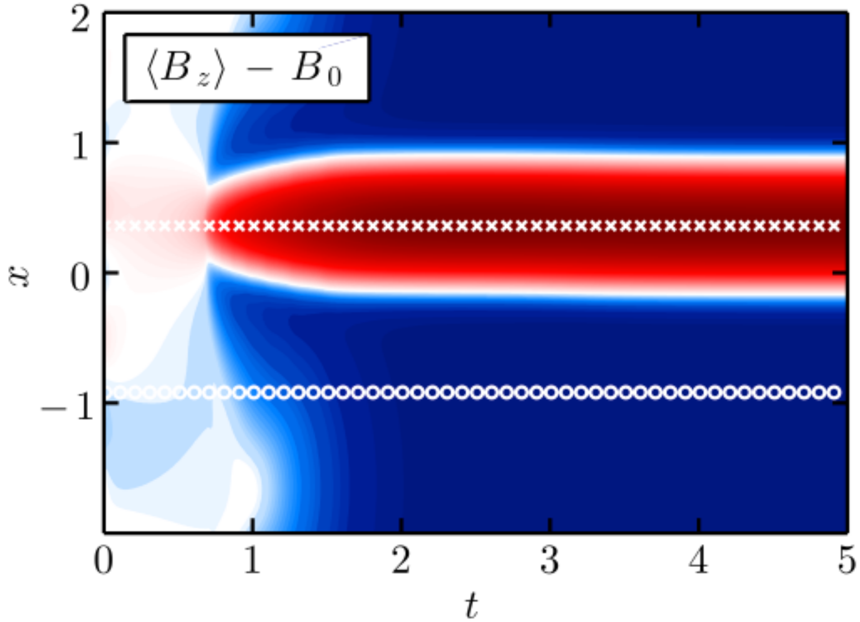

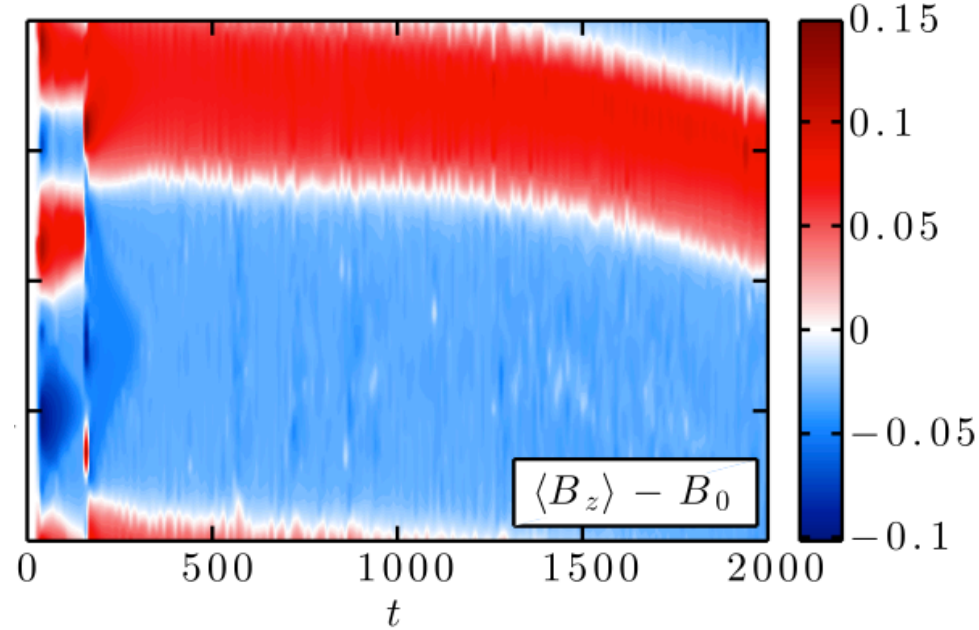

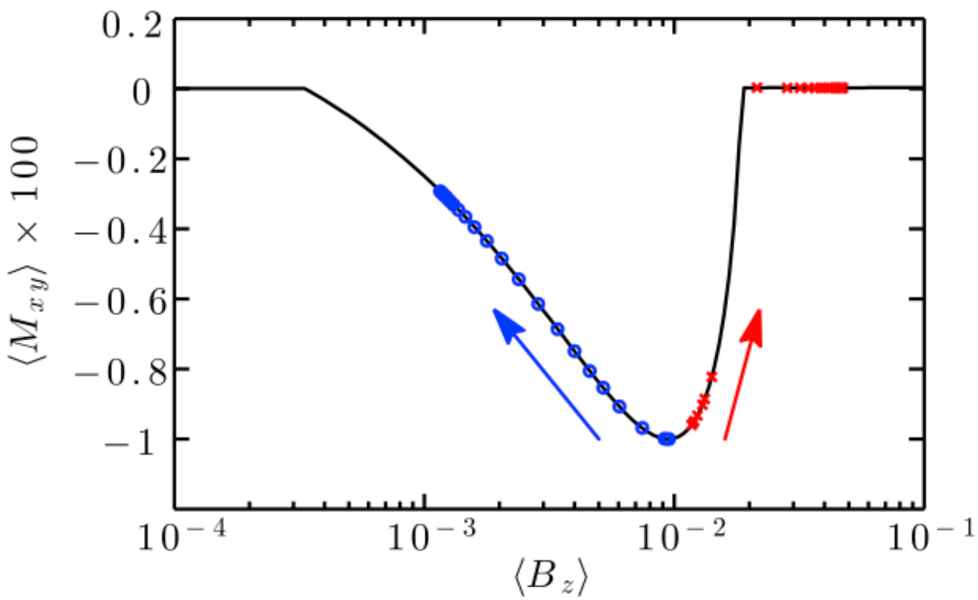

why
$\ell_{\rm H}/H \sim 0.2$?

$$\frac{c}{e n_{\rm e}} \frac{{\rm d}M}{{\rm d}\langle B_z \rangle}\bigg|_{\langle B_0 \rangle} > \eta + \eta_{\rm t}$$

$$= \ell_{\rm H} \left(\frac{4\pi}{\rho}\right)^{1/2}$$

$$\sim \frac{\alpha \rho (\Omega H)^2}{B_{z,{\rm stab}}}$$

$$\sim \frac{\alpha \Omega H^2}{{\rm Pm}_{\rm t}}$$

$$\sim 2$$

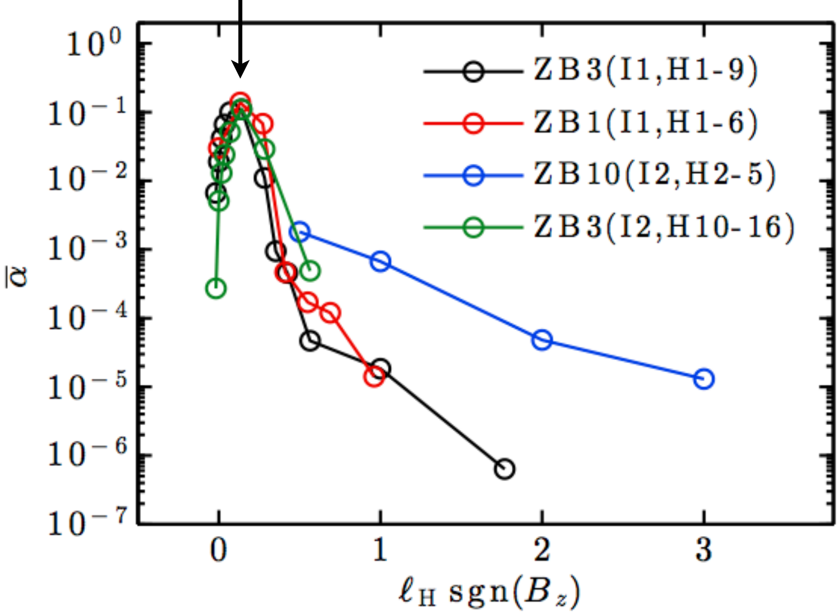

$$\boxed{\ell_{\rm H} \gtrsim \frac{v_{\rm A,stab}}{\Omega\, {\rm Pm}_{\rm t}} \sim 0.2H}$$

Case II: $\langle M_{xy} \rangle = M(\langle B_z \rangle, \underbrace{\langle \omega_z \rangle}_{\langle \omega_z \rangle = \frac{\partial \langle v_y \rangle}{\partial x} + 2A})$

$$\frac{\partial \langle B_z \rangle}{\partial t} \simeq \left(\eta + \eta_{\mathrm{t}} - \frac{c}{e n_{\mathrm{e}}} \frac{\mathrm{d}M}{\mathrm{d}\langle B_z \rangle} \right) \frac{\partial^2 \langle B_z \rangle}{\partial x^2} \boxed{- \frac{c}{e n_{\mathrm{e}}} \frac{\partial M}{\partial \langle \omega_z \rangle} \frac{\partial^2 \langle \omega_z \rangle}{\partial x^2}}$$

$$\frac{\partial \langle \omega_z \rangle}{\partial t} \simeq \left(\nu + \nu_{\mathrm{t}} + \frac{1}{\rho} \frac{\mathrm{d}M}{\mathrm{d}\langle \omega_z \rangle} \right) \frac{\partial^2 \langle \omega_z \rangle}{\partial x^2} \boxed{+ \frac{1}{\rho} \frac{\partial M}{\partial \langle B_z \rangle} \frac{\partial^2 \langle B_z \rangle}{\partial x^2}}$$

mean-field model simulation results

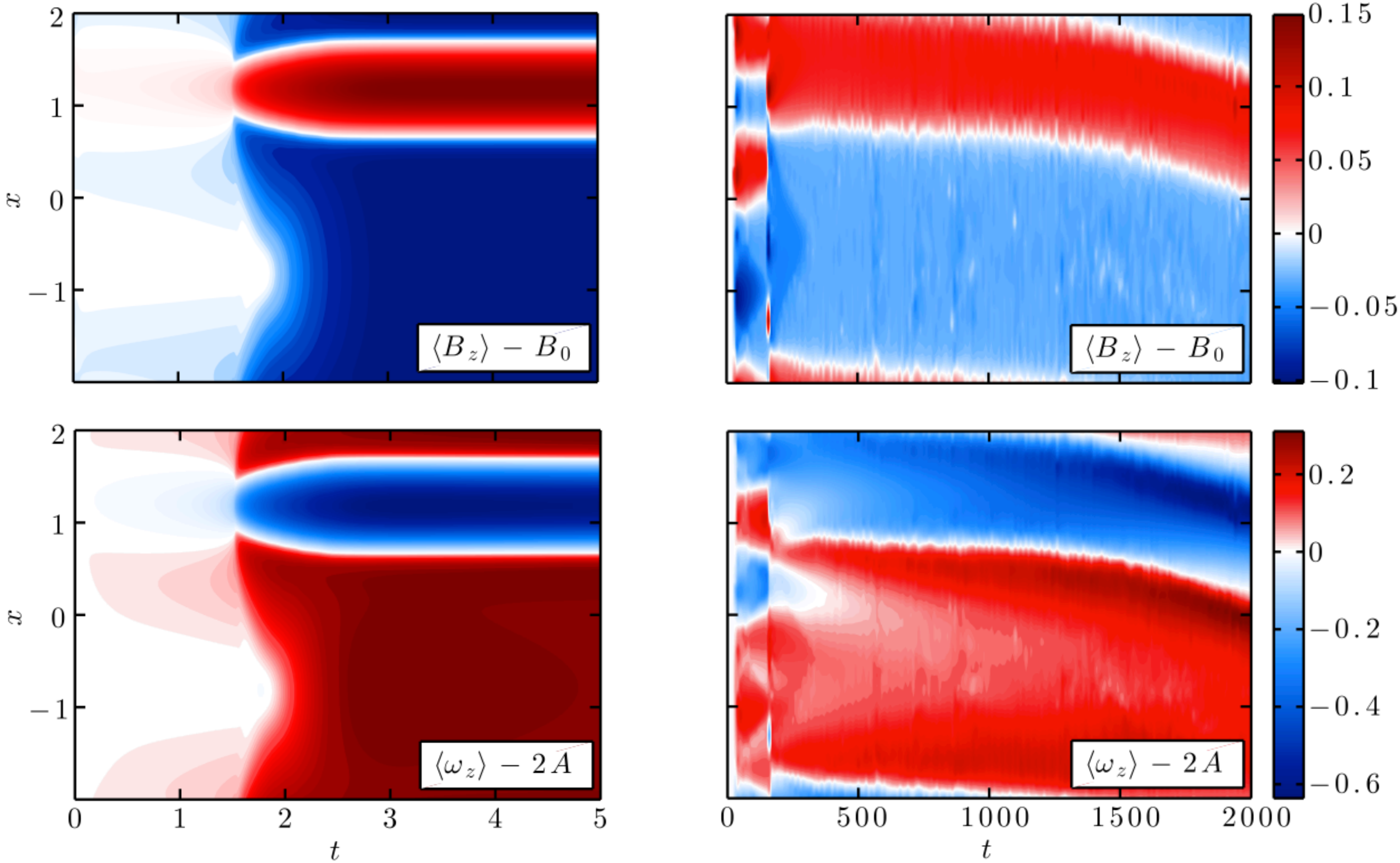

conservation of canonical vorticity

dust trapping in zonal flows

zonal magnetic field $\dfrac{eB_0}{mc}\dfrac{n_\mathrm{e}}{n}\left(1-\dfrac{\langle B_z\rangle}{B_0}\right)$

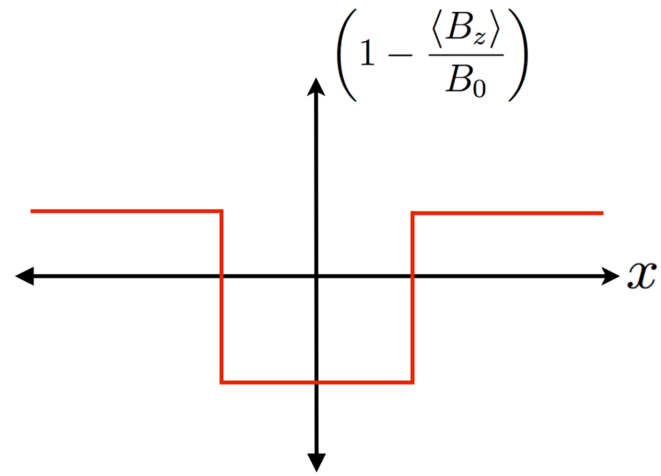

conservation of canonical vorticity $=\langle\omega_z\rangle-2\Omega\left(1+\dfrac{A}{\Omega}\right)$

def'n of vorticity $=\dfrac{\partial\langle v_y\rangle}{\partial x}$

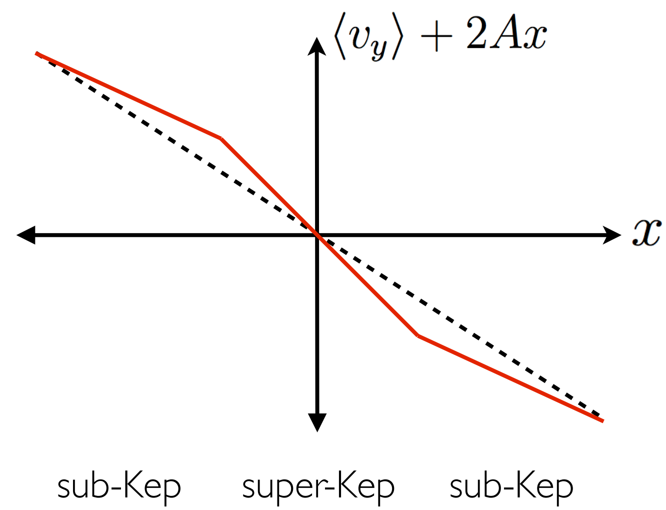

geostrophic balance for gas $=\dfrac{1}{\rho}\dfrac{\partial^2\langle P\rangle}{\partial x^2}$

...but dust is pressure-less

zonal field ⟶ zonal flow ⟶ particle clumping

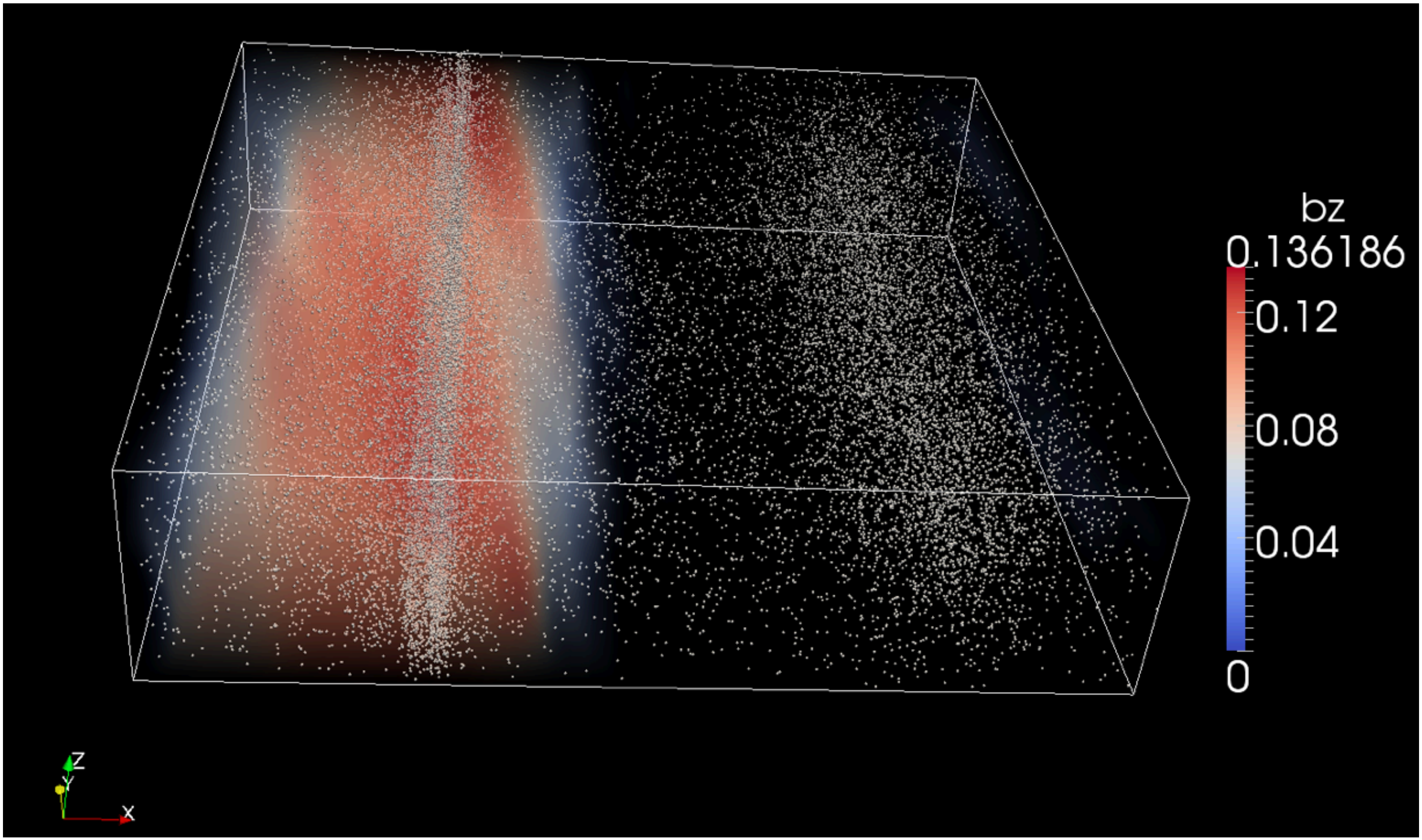

does AD affect self-organization?

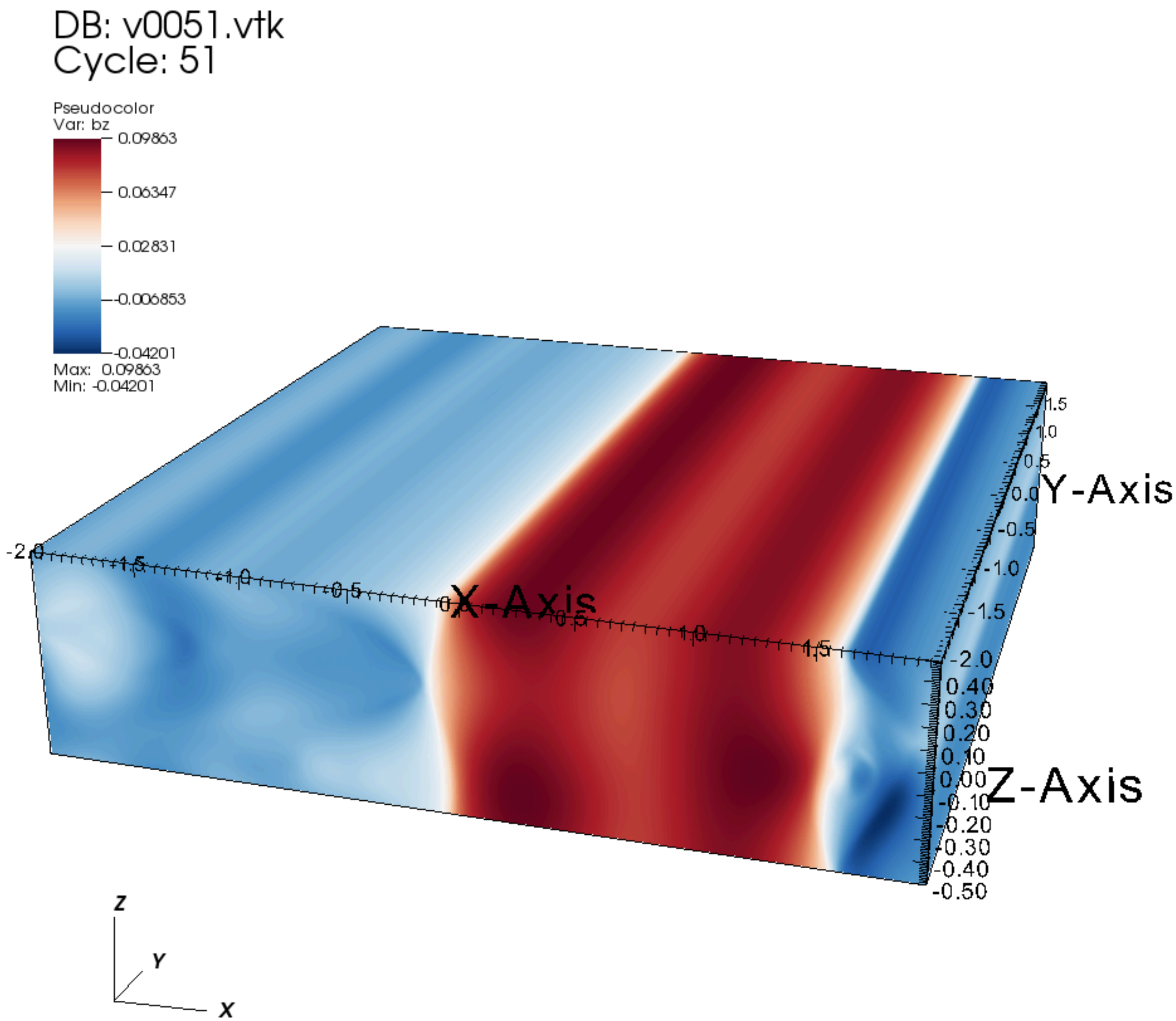

$\ell_{\rm H}$ 0.97

β 1000

Am 1

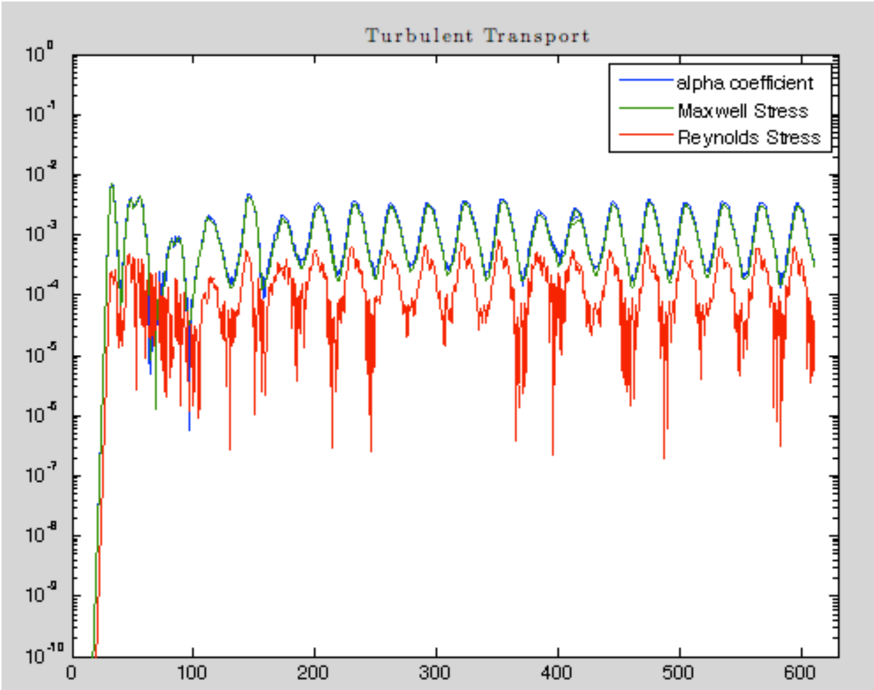

Am 1

ℓ_H 0.55

β 1000

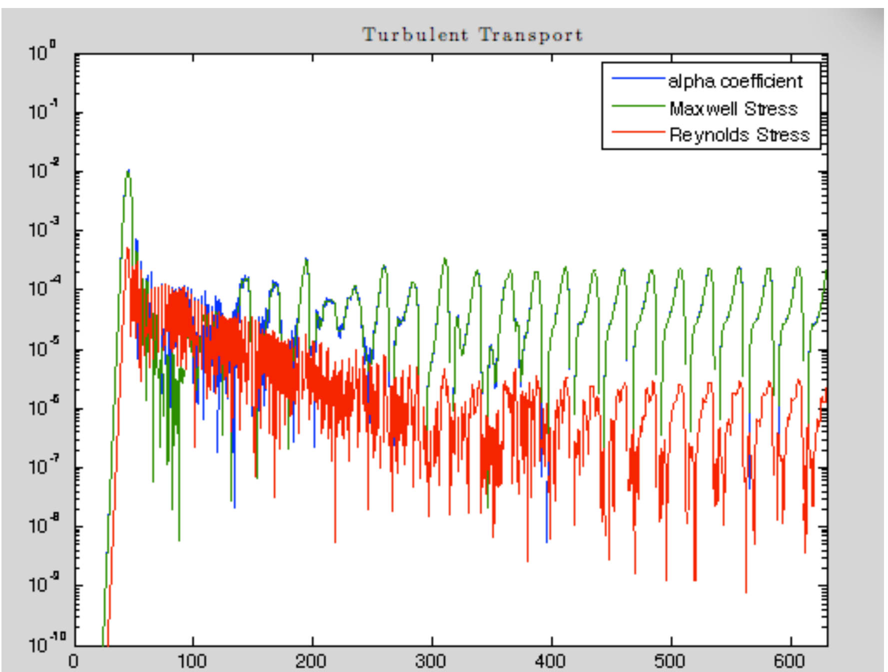

ℓ_H 0.97

β 1000

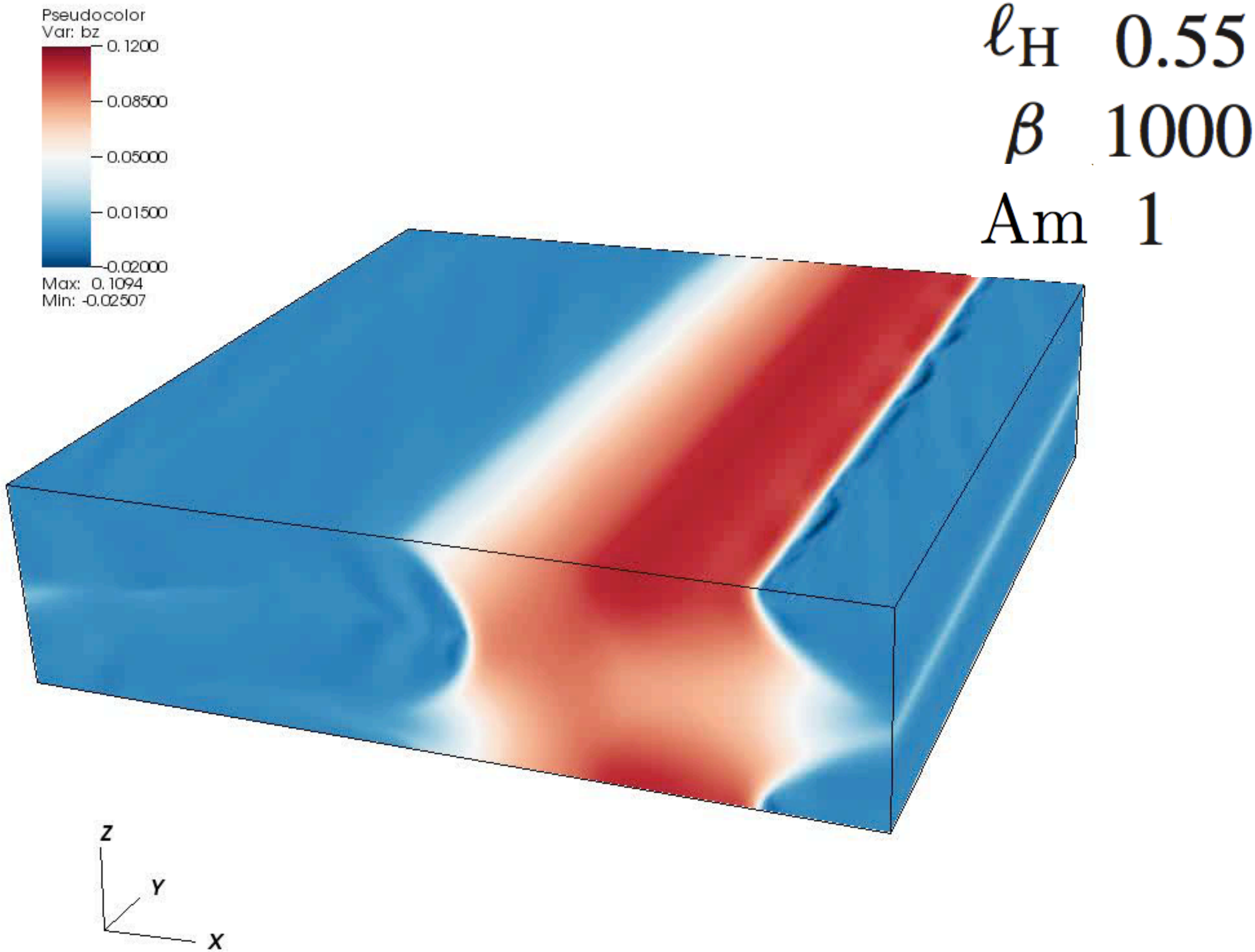

Pseudocolor
Var: bz
0.1200
0.08500
0.05000
0.01500
-0.02000
Max: 0.1094
Min: -0.02507
ℓ_H 0.55
β 1000
Am 1
Z
Y
X

$$\frac{\partial \langle B_z^1 \rangle}{\partial t} \simeq \underbrace{\left(\eta + \eta_{\mathrm{t}} + \frac{\langle v_{\mathrm{A}}^2 \rangle}{\gamma \rho_{\mathrm{i}}} - \frac{c}{e n_{\mathrm{e}}} \frac{\mathrm{d}M}{\mathrm{d}\langle B_z \rangle} \right)_{\langle B_z^0 \rangle}} \frac{\partial^2 \langle B_z^1 \rangle}{\partial x^2}$$

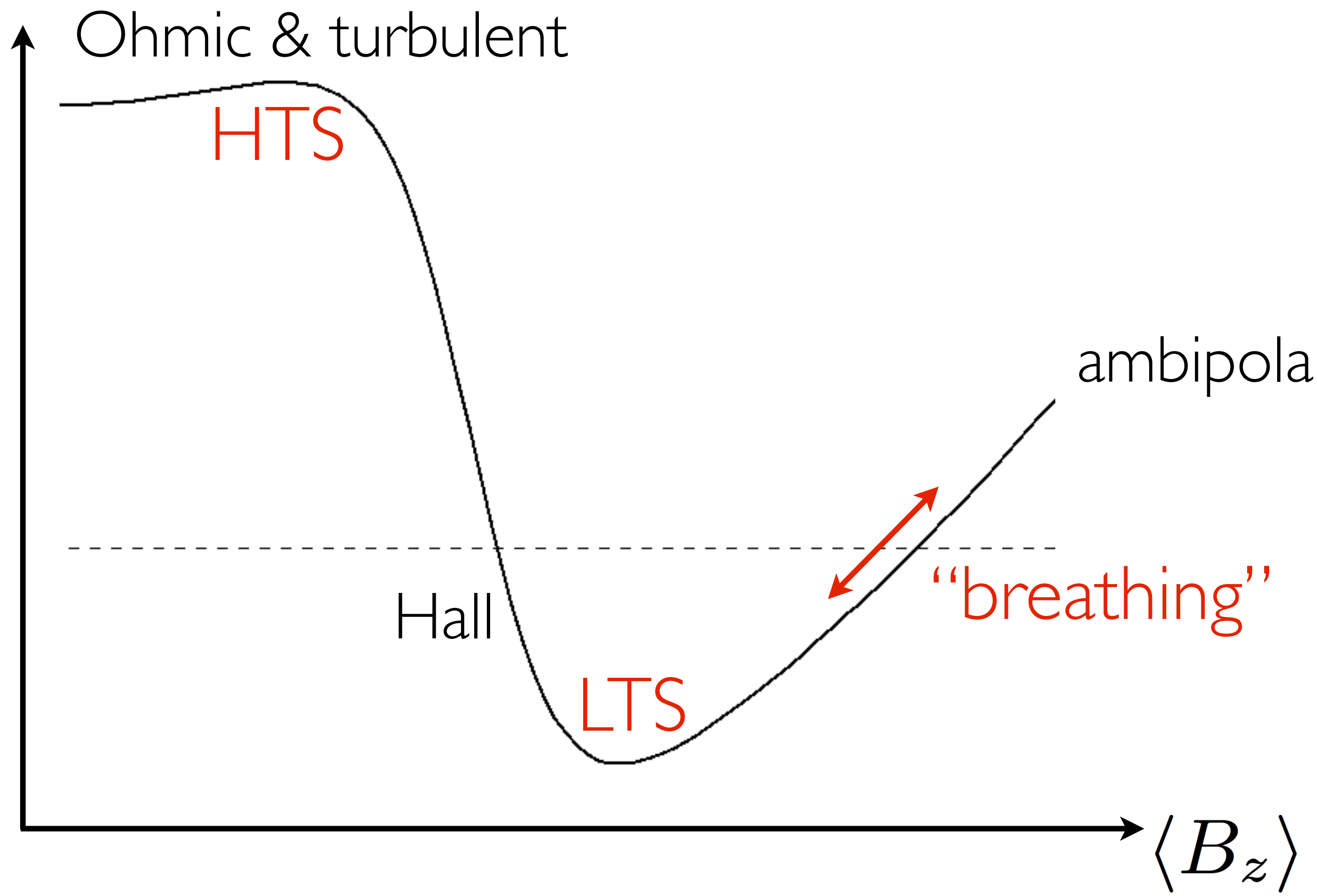

NB: this behavior is not seen in By >> Bz boxes

must know field geometry!

Summary & Outlook

- Non-ideal MHD important in PPDs.
  Hall dominates around r ~ 5 - 10 au.
- Linear analysis –> Hall could eliminate (or at least shrink) dead zone. Old simulations predict negligible change in MRI with Hall.
- When By ~< Bz, Hall-dominated regions saturate in low-transport state, exhibiting long-lived zonal magnetic fields and flows.
- These regions are MRI “dead” even though they are magnetically “active”, calling into question previous estimates for dead zone.
- Zonal structures may act as particle-trapping sites; magnetically mediated planetesimal formation a possibility.
- Stratified simulations with OD, AD, Hall have been published; stay for Geoffroy’s talk!

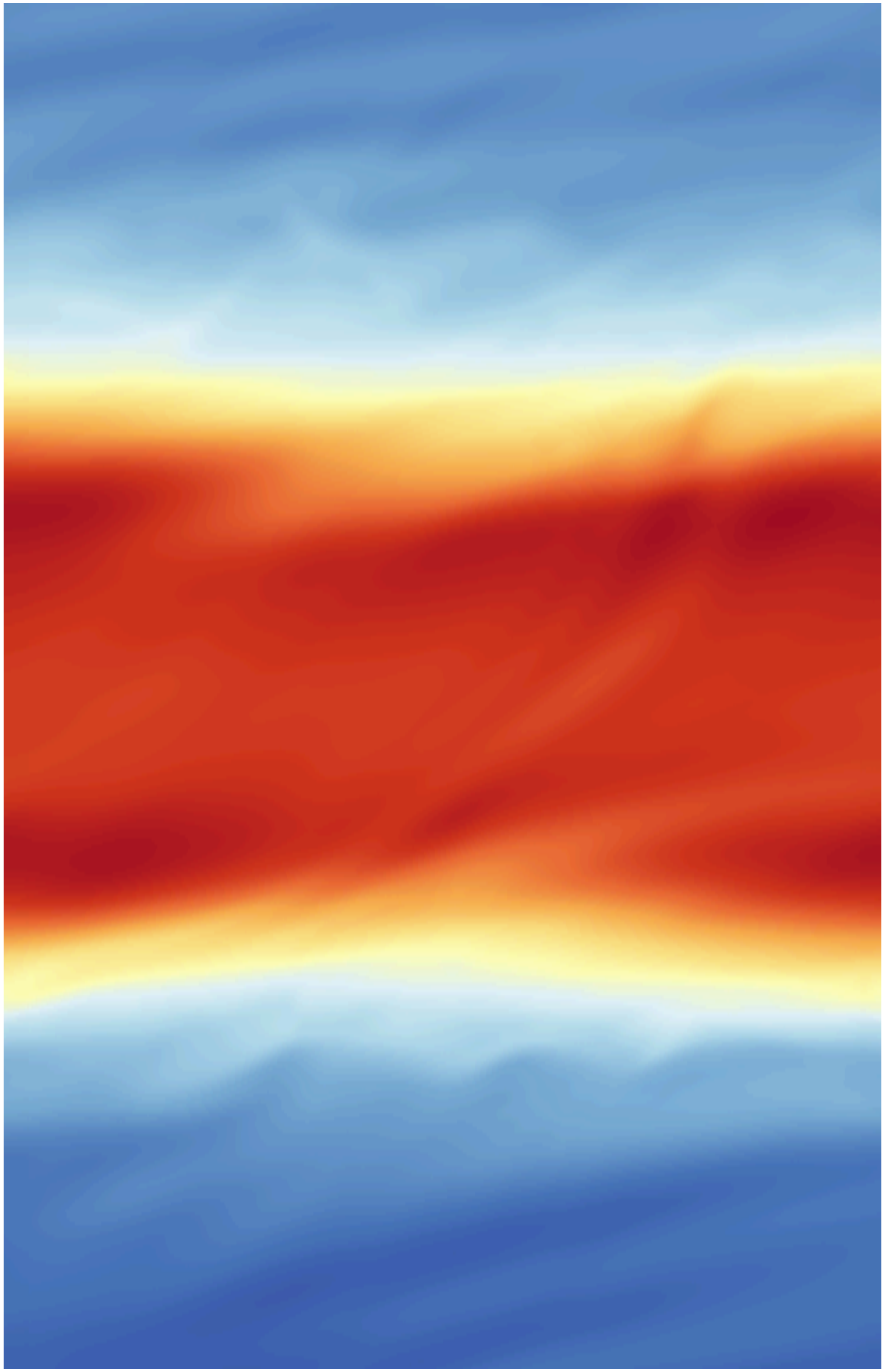

extras

parasite analysis

$$\boldsymbol{v} = \boldsymbol{v}_{\rm ch} + \delta\boldsymbol{v}, \quad \boldsymbol{B} = \boldsymbol{B}_{\rm ch} + \delta\boldsymbol{B}, \quad P = P_0 + \delta P$$

$$\begin{aligned} \boldsymbol{B}_{\rm ch} &= b e^{\gamma t} B_0 \cos Kz \, (\hat{\boldsymbol{e}}_x \sin\theta - \hat{\boldsymbol{e}}_y \cos\theta) \\ \boldsymbol{v}_{\rm ch} &= b e^{\gamma t} v_0 \sin Kz \, (\hat{\boldsymbol{e}}_x \cos\phi + \hat{\boldsymbol{e}}_y \sin\phi) \end{aligned}$$

$$\delta \propto \exp(\sigma t + {\rm i}\boldsymbol{k}\cdot\boldsymbol{x})$$

$$\boldsymbol{k} = k \, (\hat{\boldsymbol{e}}_x \sin\theta_k - \hat{\boldsymbol{e}}_y \cos\theta_k)$$

$$\begin{aligned} \sigma\delta\boldsymbol{v} = &-{\rm i}\boldsymbol{k}\cdot\boldsymbol{v}_{\rm ch}\,\delta\boldsymbol{v} - \delta v_z \frac{{\rm d}\boldsymbol{v}_{\rm ch}}{{\rm d}z} - \frac{1}{\rho}\left({\rm i}\boldsymbol{k} + \hat{\boldsymbol{e}}_z \frac{\rm d}{{\rm d}z}\right)\delta\Pi \\ &+ {\rm i}\boldsymbol{k}\cdot\boldsymbol{B}_{\rm ch}\frac{\delta\boldsymbol{B}}{4\pi\rho} + \frac{\delta B_z}{4\pi\rho}\frac{{\rm d}\boldsymbol{B}_{\rm ch}}{{\rm d}z} + \nu\left(\frac{{\rm d}^2}{{\rm d}z^2} - k^2\right)\delta\boldsymbol{v}, \end{aligned} \tag{A1}$$

$$\begin{aligned} \sigma\delta\boldsymbol{B} = &-{\rm i}\boldsymbol{k}\cdot\left(\boldsymbol{v}_{\rm ch} - \frac{\boldsymbol{J}_{\rm ch}}{e n_{\rm e}}\right)\delta\boldsymbol{B} - \left(\delta v_z - \frac{\delta J_z}{e n_{\rm e}}\right)\frac{{\rm d}\boldsymbol{B}_{\rm ch}}{{\rm d}z} \\ &+ {\rm i}\boldsymbol{k}\cdot\boldsymbol{B}_{\rm ch}\left(\delta\boldsymbol{v} - \frac{\delta\boldsymbol{J}}{e n_{\rm e}}\right) + \delta B_z \frac{\rm d}{{\rm d}z}\left(\boldsymbol{v}_{\rm ch} - \frac{\boldsymbol{J}_{\rm ch}}{e n_{\rm e}}\right) \\ &+ \eta\left(\frac{{\rm d}^2}{{\rm d}z^2} - k^2\right)\delta\boldsymbol{B}, \end{aligned} \tag{A2}$$

$${\rm i}\boldsymbol{k}\cdot\delta\boldsymbol{v} + \frac{{\rm d}\delta v_z}{{\rm d}z} = 0, \tag{A3}$$

where

$$\delta\Pi = \delta P + \frac{\boldsymbol{B}_{\rm ch}\cdot\delta\boldsymbol{B}}{4\pi}$$

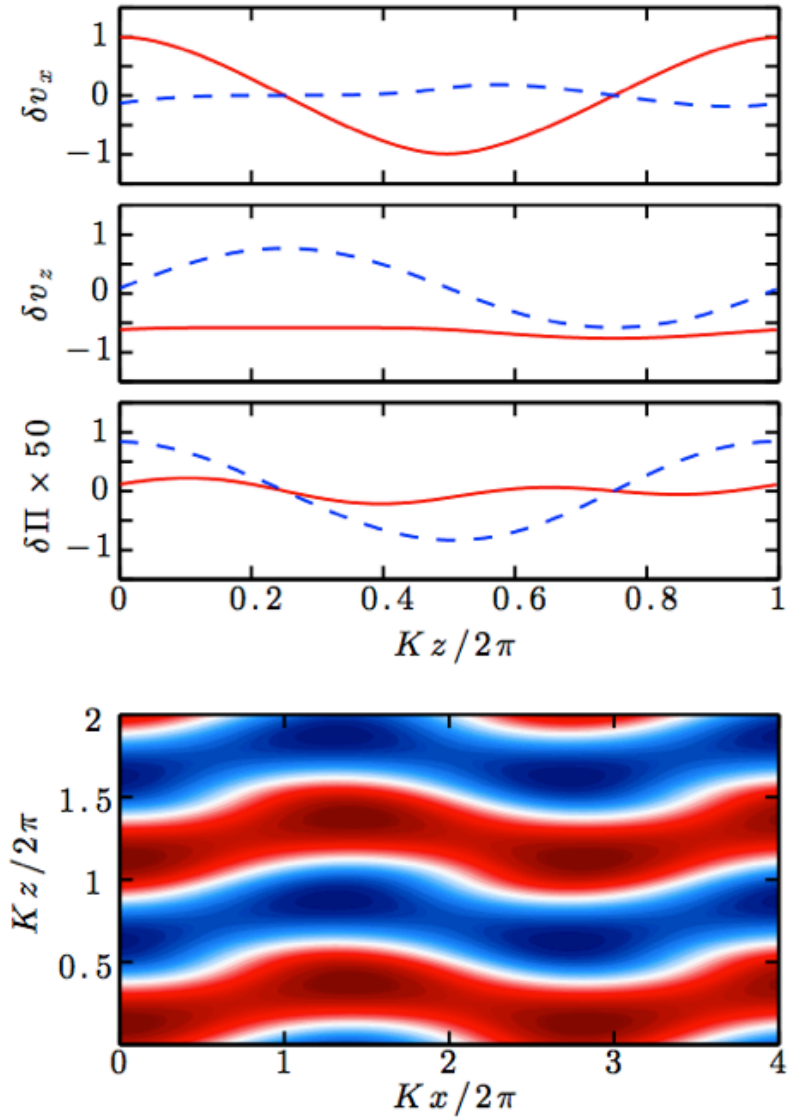

Figure A1. (*top*) The δv_x, δv_z, and $\delta\Pi$ components of the eigenfunction of a kink mode with $\theta = \phi = \pi/4$, $k/K = 0.5$, $\theta_k = -\pi/4$, and $k_z = 0$. The solid (dashed) lines denote the real (imaginary) parts. The total eigenfunction is normalised so that $\max|\delta v_x| = 1$. The growth rate $\sigma/b\Omega = 0.008616$. (*bottom*) Coloured iso-contours of the real part of v_x at $y = 0$ in the (x, z) plane. The background is a four-stream Hall-MRI channel with jets centred at $Kz = n\pi/2$ with $n = 1,\ 3,\ 5$ and 7. The perturbation is normalised so that $\max|\delta v_x| = v_{\rm ch}$.

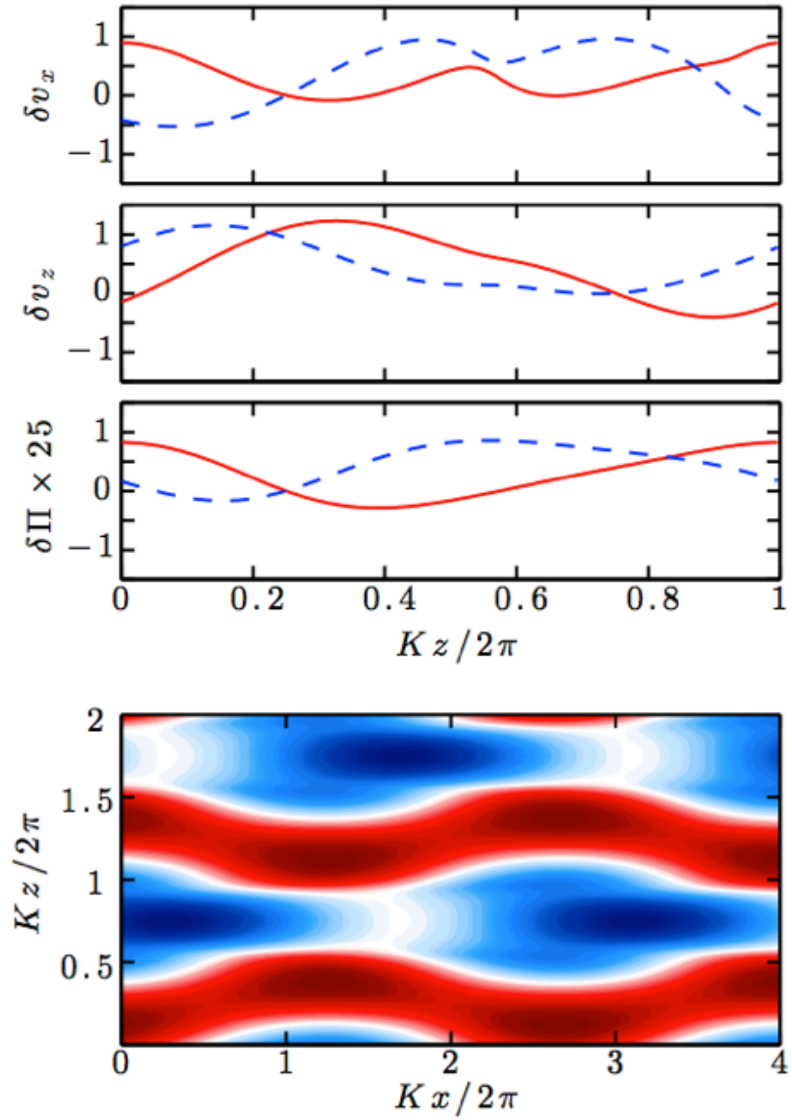

Figure A2. (*top*) The δv_x, δv_z, and $\delta\Pi$ components of the eigenfunction of a kink-pinch mode with $\theta = \phi = \pi/4$, $k/K = 0.5$, $\theta_k = -\pi/4$, and $k_z = 0.5$. The solid (dashed) lines denote the real (imaginary) parts. The total eigenfunction is normalised so that $\max|\delta v_x| = 1$. The growth rate $\sigma/b\Omega = 0.004093 + 0.0058\mathrm{i}$. (*bottom*) Coloured iso-contours of the real part of v_x at $y = 0$ in the (x, z) plane. The background channel and normalisation are as in Figure A1. The entire pattern is moving to the left because σ possesses a positive imaginary part.

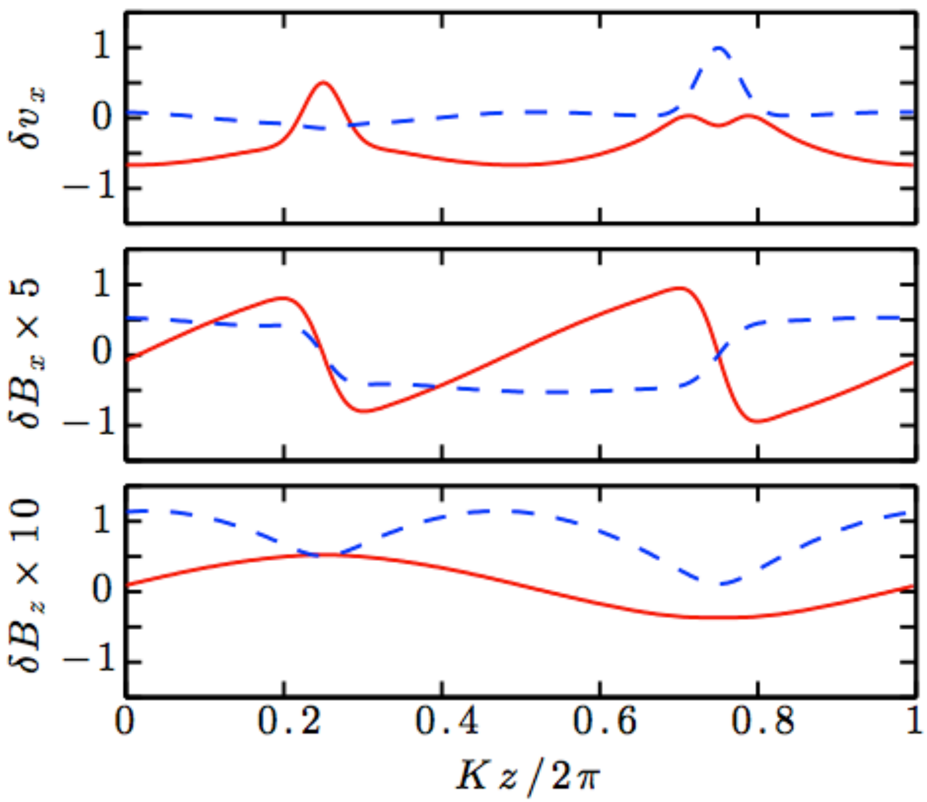

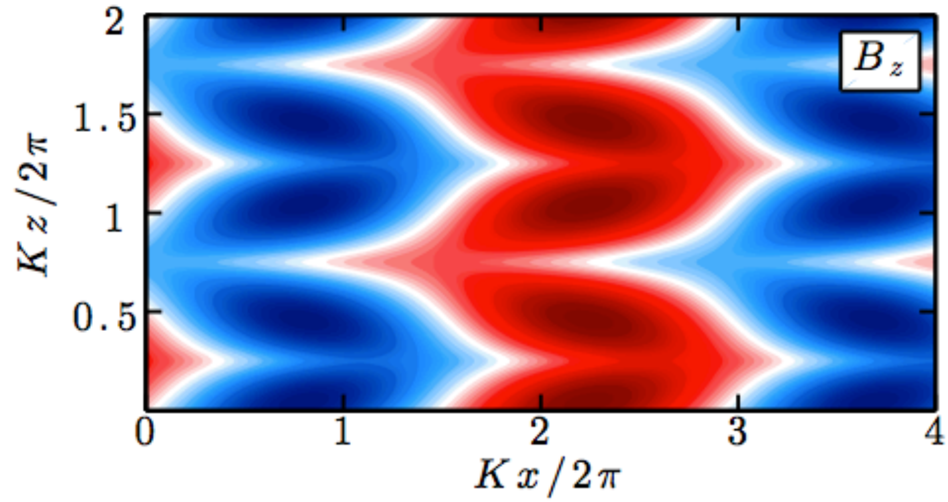

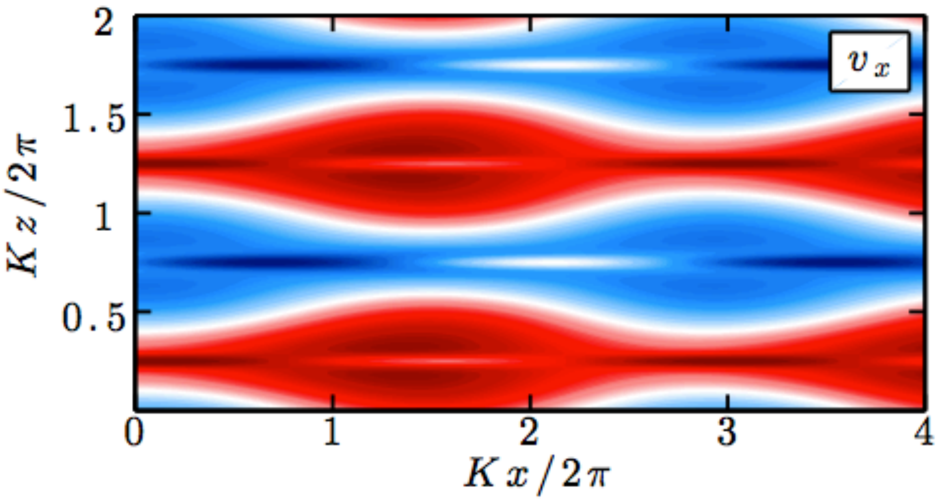

Figure A3. (*top*) The δv_x, δB_x, and δB_z components of the eigenfunction of a pinch-tearing mode with $\theta_k = \pi/3$, $k/K = 0.4$, $k_z = 0$, and $b = 5$. The channel orientation $\theta \simeq 0.255\pi$ is obtained by solving the dispersion relation for the fastest-growing mode with β, $\Lambda_{\rm H}$, and Λ_η taken from our fiducial simulation ZB1H1. The solid (dashed) line denotes the real (imaginary) part. The total eigenfunction is normalised so that $\max|\delta v_x| = 1$. The growth rate $\sigma/b\Omega = 0.02868 - 0.03449$i. (*bottom*) Coloured isocontours of the real parts of v_x and B_z at $y = 0$ in the (x, z) plane. The background channel and normalisation are as in Figure A1. The entire pattern is moving to the right because σ possesses a negative imaginary part.

The HSI is most easily examined in the limit of negligible resistivity, in which case the channel magnetic and velocity fields are mutually perpendicular ($\theta = \phi$; see eq. 17). We can therefore erect an orthonormal coordinate system oriented with the channel mode: $\hat{\boldsymbol{e}}_b = \boldsymbol{B}_{\rm ch}/B_{\rm ch}$, $\hat{\boldsymbol{e}}_v = \boldsymbol{v}_{\rm ch}/v_{\rm ch}$, and $\hat{\boldsymbol{e}}_z = \hat{\boldsymbol{e}}_b \times \hat{\boldsymbol{e}}_v$. In this geometry, wavevectors parallel to the channel magnetic field ($\boldsymbol{k} = k\hat{\boldsymbol{e}}_b$) have the greatest potential for growth. The z- and v-components of the linearised induction equation (A2) become[9]

$$\sigma\delta B_z - b\cos Kz\,\frac{ck^2B_0}{4\pi e n_{\rm e}}\,\delta B_v = {\rm i}kB_0\,b\cos Kz\,\delta v_z, \tag{A4}$$

$$\sigma\delta B_v + b\cos Kz\left[\frac{ck^2B_0}{4\pi e n_{\rm e}}\left(1 - \frac{1}{k^2}\frac{{\rm d}^2}{{\rm d}z^2} - \frac{K^2}{k^2}\right) - Kv_0\right]\delta B_z$$
$$= {\rm i}kB_0\,b\cos Kz\,\delta v_v. \tag{A5}$$

It is clear from equation (A5) that the shear of the channel mode (represented by the final term in the brackets) uses δB_z to generate δB_v. The Hall terms, on the other hand, generate δB_z at the expense of δB_v. This effect is present even in the absence of shear and arises because the v-component of the perturbed electron velocity differs from the ion-neutral velocity by

$$-\frac{\delta J_v}{e n_{\rm e}} = \frac{{\rm i}ck}{4\pi e n_{\rm e}}\left(1 - \frac{1}{k^2}\frac{{\rm d}^2}{{\rm d}z^2}\right)\delta B_z.$$

The induced magnetic field is sheared further, and there is the potential for runaway.

It is a straightforward exercise to show from equations (A1), (A4), and (A5) that, whether $k \gg K, {\rm d}/{\rm d}z$ (the limit captured by the K08 analysis) or ${\rm d}/{\rm d}z \gg k, K$ (a WKBJ treatment), a necessary condition for instability is

$$1 < \frac{Kv_0}{\omega_{\rm H,0}}. \tag{A6}$$

Physically, this inequality states that the time required from an ion to execute one orbital gyration around a magnetic-field line must be longer (by a factor of $n_{\rm e}/n$) than the time it takes for a magnetic perturbation to grow by shear. If this condition is not met, the ions are well-coupled to the electrons (and thereby to the magnetic field), and we are left with simple linear-in-time growth due to shearing of the magnetic-field perturbation by the channel flow.

APPENDIX B: NUMERICAL STABILITY IN HALL-MHD

Falle (2003) suggested that explicit schemes for numerically solving the equations of Hall-MHD are unconditionally unstable due to the existence of small-wavelength whistler waves. Although this conclusion is correct for the numerical schemes Falle (2003) considered, here we demonstrate that *higher order* time-explicit schemes, such as the one used in SNOOPY, are stable without the need for physical (e.g. Ohmic or ambipolar) or artificial (e.g. hyper-resistive) wave damping.

We start by considering the induction equation (equation 2) with the first (ideal) and third (Ohmic) terms on the right-hand side dropped. Decomposing the magnetic field into a fixed guide field $\boldsymbol{B}_0$ and a small-amplitude fluctuation $\delta\boldsymbol{B}(t)\exp(\mathrm{i}\boldsymbol{k}\cdot\boldsymbol{x})$, we find that linear whistler waves are described by

$$\frac{\mathrm{d}\delta\boldsymbol{B}}{\mathrm{d}t} = \frac{c\boldsymbol{k}\cdot\boldsymbol{B}_0}{4\pi e n_e}\,(\boldsymbol{k}\times\delta\boldsymbol{B})\,. \tag{B1}$$

In spectral codes such as SNOOPY the right-hand side of this equation is computed exactly using Fourier decomposition, and we adopt this scheme in what follows.

Without loss of generality we take the wavevector $\boldsymbol{k} = k\hat{\boldsymbol{e}}_z$ and magnetic-field perturbation $\delta\boldsymbol{B} = \delta B_x\hat{\boldsymbol{e}}_x + \delta B_y\hat{\boldsymbol{e}}_y$, ensuring $\boldsymbol{k}\cdot\delta\boldsymbol{B} = 0$. Equation (B1) can then be written as

$$\frac{\mathrm{d}\delta\boldsymbol{B}}{\mathrm{d}t} = \mathbf{R}\,\delta\boldsymbol{B}, \quad \text{where} \quad \mathbf{R} \equiv \frac{ck^2B_{0,z}}{4\pi e n_e}\begin{pmatrix} 0 & -1 \\ 1 & 0 \end{pmatrix}. \tag{B2}$$

We integrate equation (B2) forward in time from $t^{(n)}$ to $t^{(n+1)}$ using an RK3 scheme similar to that used in SNOOPY. For a system of differential equations $\boldsymbol{y}' = \boldsymbol{f}(\boldsymbol{y})$, this procedure reads

$$\begin{aligned}
\boldsymbol{q}_1 &= \boldsymbol{f}\left(\boldsymbol{y}^{(n)}\right) \\
\boldsymbol{q}_2 &= \boldsymbol{f}\left(\boldsymbol{y}^{(n)} + \frac{h}{2}\boldsymbol{q}_1\right) \\
\boldsymbol{q}_3 &= \boldsymbol{f}\left(\boldsymbol{y}^{(n)} - h\boldsymbol{q}_1 + 2h\boldsymbol{q}_2\right) \\
\boldsymbol{y}^{(n+1)} &= \boldsymbol{y}^{(n)} + \frac{h}{6}(\boldsymbol{q}_1 + 4\boldsymbol{q}_2 + \boldsymbol{q}_3),
\end{aligned}$$

where $h \equiv t^{(n+1)} - t^{(n)}$. Applying this algorithm to equation (B2), we find

$$\delta\boldsymbol{B}^{(n+1)} = \mathbf{Q}\,\delta\boldsymbol{B}^{(n)} \tag{B3}$$

for

$$\mathbf{Q} = \begin{pmatrix} 1-\frac{1}{2}\varepsilon^2 & -\varepsilon+\frac{1}{6}\varepsilon^3 \\ \varepsilon-\frac{1}{6}\varepsilon^3 & 1-\frac{1}{2}\varepsilon^2 \end{pmatrix} \quad \text{and} \quad \varepsilon \equiv h\,\frac{ck^2B_{0,z}}{4\pi e n_e}.$$

Note that the matrix $\mathbf{Q}$ is a third-order expansion of the formal solution $\delta\boldsymbol{B}^{(n+1)} = \exp(h\mathbf{R})\,\delta\boldsymbol{B}^{(n)}$. Extensions to higher order are straightforward.

Stability is guaranteed if the eigenvalues of $\mathbf{Q}$,

$$\lambda_{\pm} = 1 - \frac{\varepsilon^2}{2} \mp \mathrm{i}\left(\varepsilon - \frac{\varepsilon^3}{6}\right),$$

satisfy the inequality $|\lambda_{\pm}| < 1$. The numerical scheme is therefore stable provided $\varepsilon < \sqrt{3}$; SNOOPY uses $\varepsilon = 1.5$. It can easily be shown by this approach that similar schemes of first or second order in time, such as the ones considered by Falle (2003), are unconditionally unstable. The fourth-order Runge–Kutta scheme is stable for $\varepsilon < 2\sqrt{2}$.

In conclusion, the third-order explicit time integrator employed in SNOOPY guarantees that linear whistler waves are stable, without the need for additional diffusion terms.

This paper has been typeset from a TEX/LATEX file prepared by the author.